FACIES	49	299-324	Pl. 45-53	4 Figs.	1 Tab.	Erlangen 2003

Shark Bay Stromatolites: Microfabrics and Reinterpretation of Origins

R. Pamela **Reid**, Miami; Noel P. **James**, Kingston; Ian G. **Macintyre**, Washington D.C.; Christophe P. **Dupraz**, Neuchâtel; Robert V. **Burne**, Canberra

KEYWORDS: STROMATOLITES – MARINE; MICROBIAL - PRECIPITATION; MICRITE; *ENTOPHYSALIS*; SHARK BAY (AUSTRALIA)

Summary

Detailed analysis of microfabrics in Hamelin Pool stromatolites leads to reinterpretation of the origins of these structures. Previous studies have concluded that Shark Bay stromatolites form primarily as a result of sediment trapping and binding by microorganisms. Our results suggest that microbial precipitation of microcrystalline carbonate (micrite), as both framework and cement in these stromatolites, is also a fundamental, heretofore unrecognized, process in their formation. Microbial trapping and binding is the primary mechanism of stromatolite accretion in the intertidal zone, forming grainy, calcarenite structures. Microbial precipitation is the primary accretionary mechanism in the subtidal zone, forming muddy, micritic stromatolites. Microbial precipitation also lithifies trapped and bound sediment in the calcarenite stromatolites. Recognition of microbially precipitated micrite in Shark Bay stromatolites is important, as many ancient stromatolites are micritic.

1 INTRODUCTION

The most abundant and diverse modern stromatolites in the modern world ocean occur in Hamelin Pool, a hypersaline embayment of Shark Bay, Western Australia (Fig. 1). These stromatolites were discovered in 1954 by D. Johnstone, P.E. Playford and R.L. Chase of West Australian Petroleum Pty. Ltd (Playford and Cockbain 1976). They were the first known modern microbial buildups with sizes and shapes analogous to Precambrian stromatolites, which dominated the fossil record for much of Earth history. As such, Hamelin Pool stromatolites have had a profound impact on stromatolite research and, for many years, they were used as a basis for comparison with all fossil examples (Playford 1979; Riding, 1991; McNamara, 1999).

Microorganisms construct stromatolites by trapping and binding sediment and/or precipitating a framework of calcium carbonate. Based on previous studies, which have emphasized the coarse grained, detrital nature of Hamelin Pool stromatolites (e.g. Logan 1961; Logan et al. 1974; Playford and Cockbain 1976), these structures are widely believed to have accreted through sediment trapping and binding (Playford 1990; Golubic 1992; McNamara 1999). Indeed, in the past decade, it has been suggested that the coarse grained Shark Bay buildups are inappropriate analogs for ancient stromatolites, which are typically composed of microcrystalline carbonate (micrite) (e.g. Awramik and Riding 1988; Riding 1994). The potential role of microbial precipitation in the accretion and lithification of Shark Bay stromatolites (Burne and Moore (1987) has received relatively little attention and, in the words of Playford (1990, p. 29), "further work needs to be done to more closely link details of the internal fabrics of the stromatolites to the microbial communities that build them".

Geomicrobiological studies linking microfabric to microbial activity have recently been applied to the study of modern Bahamian stromatolites. Detailed correlations of subsurface petrographic features, as seen in thin sections, with analysis of microbial populations and microbial processes in surface mats show the importance of prokaryotic microbial communities in the accretion, lamination and early lithification of marine stromatolites in Exuma Cays (e.g. Reid et al. 2000; Visscher et al. 1998, 2000; Kawaguchi and Decho 2001, 2002). Although Shark Bay stromatolites were discovered more than 40 years ago, previous studies have emphasized morphology in relation to environmental setting (e.g. Playford 1980) and there are very few detailed descriptions of thin sections or published photomicrographs (Monty 1976).

The aim of this paper is to provide an analysis of microfabrics in Shark Bay stromatolites. This is a critical first step in defining the role of microbial activity in stromatolite accretion and lithification.

2 BACKGROUND

2.1 Terminology

To be consistent with earlier studies (e.g. Playford 1990), the term 'stromatolite' is used in this paper for all organosedimentary structures formed by the sediment-binding and/or carbonate precipitating activities of microorganisms, re-

Addresses: P. Reid, University of Miami, 4600 Rickenbacker Causeway, Miami, FL 33149 USA; preid@rsmas.miami.edu; N. P. James, Dept. Geological Sciences, Queen's University, Kingston Ont., Canada K7L3N6; I.G. Macintyre, Smithsonian Institution, National Museum of natural History, Washington D.C., 20013, USA; C.P. Dupraz, Université de Neuchâtel, 11 Rue Emile Argand, Case Postale 2, CH-2007 Neuchâtel, Switzerland; R.V. Burne, Dept. Geology, Australian National University Canberra, ACT 0200 Australia

Fig. 1. Location map of Shark Bay, Western Australia, showing Hamelin Pool and the sampling sites at Flagpole Landing and Carbla Point. Dashed lines are roads.

gardless of whether or not they are laminated. In this usage, the term is equivalent to 'microbialite' of Burne and Moore (1987). We use the term 'micrite' formicrocrystalline carbonate, < 4 μm in size, without regard to mineralogy or inferred origin.

2.2 Setting

Stromatolites cover ~100 km of shoreline to water depths of 3-4 meters around the margins of Hamelin Pool, a hypersaline embayment at the southern end of Shark Bay (Fig. 1). The environment is well-documented by Logan and Cebulski (1970) and Logan et al. (1974). In general, Hamelin Pool (Fig. 1) is a shallow (<10 m deep) broad embayment, surrounded on three sides by strandline environments ranging from rocky headlands to beaches to wide intertidal flats. Hamelin Pool is separated from most of Shark Bay by a grass bank, called the Faure Sill, which impedes water circulation. Salinities range from 55-70‰ throughout the year (Playford 1990). The stromatolites are believed to have developed because of these elevated salinities, which restrict the growth of microbial grazers (cf. Garrett 1970) and other organisms that compete for the same ecological niches (cf. Monty 1973). The tidal range is 1–1.5 m; tides are mainly wind driven and are not predictable (Playford 1990).

The environment over the last 2700 years (Chivas et al. 1990) has been shallow and energetic. Today southerly winds prevail with maximum velocity of 45km/hr; cyclonic winds up to 180km/hr occur approximately once every 6 years. The domal to columnar stromatolites are found from the supratidal to shallow subtidal settings. They are developed on hard substrates in carbonate sand. Substrates are either hardgrounds or fragments of Pleistocene to Miocene limestone. Sediment in the stromatolites is mainly ooids, bivalves (including large *Fragum* shells) and benthic foraminfers, with minor detrital quartz and dolomite. Stromatolite growth is restricted to the last 4,000 years, during which time sea level receded from ~1–2m above its present level (Logan et al. 1970; Hagan and Logan 1974).

2.3 Previous Work

Previous studies (e.g. Logan et al. 1974; Playford and Cockbain 1976; Hoffman 1976; Playford 1990) recognize three types of living stromatolites at Hamelin Pool based on macroscopic descriptions of internal structures and position relative to sea level (Fig. 2). Construction of these stromatolites has been attributed to three mat types: pustular, smooth, and colloform. Each mat type has a characteristic microbial assemblage whose distribution is tidally controlled. Reported scenarios of stromatolite construction are as follows:

Upper to mid intertidal zone: Pustular mats (mamillate mats of Golubic 1983, 1992) form large columns and mounds up to 1 m wide and 40 cm high. These buildups are unlaminated,

with irregular coarse fenestral networks and irregular outer surfaces (Logan et al. 1974; Playford 1990). The pustular mats, which have a characteristic brown color, are dominated by the coccoid cyanobacterium *Entophysalis major*. The brown color results from the presence of scytonemine, a light induced extracellular pigment that is embedded in polysaccharide gel envelopes surrounding the cells. *Entophysalis major* is thought to be a descendent of the Precambrian stromatolite-building cyanobacterium *Eoentophysalis* (Golubic 1976, 1983). *E. major* mats at Hamelin Pool function as sediment traps, overgrowing and incorporating sand and silt that accumulates in their irregular surfaces (Logan et al. 1974; Golubic 1983).

Rapid lithification of pustular mats was documented by Golubic and colleagues during the peak of the austral summer in 1980 (Golubic 1983, 1992). Lithification occurs as a result of precipitation of $CaCO_3$ within the polysaccharide envelopes surrounding *E.major* cells. Pockets of shriveled cells can be found encased within the precipitates, which retain the characteristic golden to red-brown color of the live mats. SEM observations show that the gel precipitates have a globular morphology that is characteristic of amorphous carbonate formed in biological systems (Golubic 1983, 1992). These amorphous precipitates are in turn coated with abiotic crusts of aragonite needle cement.

Mature, desiccated columns in the upper intertidal to supratidal zones may be colonized by dark colored, film mats (Logan et al. 1974; Golubic, 1992). Logan et al. (1974, p. 150) described these mats as 'ecomorphs of pustular mats', comprised of 1 to 2 mm thick pelletoid rinds colonized by desiccated *E. major*. Golubic (1992) reported that the film mats were dominated by the endolithic cyanobacteria *Hormathonema luteobrunneum* and *H. violaceonigrum*, which penetrate and weaken the stromatolites (Golubic 1992). Playford and Cockbain (1976) suggested that these desiccated structures were no longer active, having died as a result of emergence due to Holocene uplift.

Lower intertidal and shallowest subtidal zones: Smooth mats construct smaller stromatolite columns and mounds. These structures are well laminated, with fine laminoid fenestral fabrics and smooth outer surfaces (Playford 1990). The smooth mats are dominated by filamentous cyanobacteria; major species are reported as *Schizothrix helva* (Logan et al. 1974, Hoffman 1976) or *Microcoleus chthonoplastes* (Bauld 1984; Golubic 1985; Golubic 1992). Stromatolite accretion results from the trapping and binding of sediment by the filamentous cyanobacteria.

Lamination was thought to be related to variation in sediment influx, with stabilization of sediment by precipitation of aragonite cement during periods of desiccation when interstitial water evaporated (Logan et al. 1974). During these exposure periods, Logan et al. (1974) reported that *Schizothrix* reverts to a boring role, producing pellets and micro-unconformities. Fenestrae develop after burial by oxidation of the mat (Logan et al. 1974). These laminated structures have been considered true stromatolites in the original sense of Kalkowsky (1908).

Subtidal zone: Colloform mats form elliptical to circular columns and compound masses from a few centimeters to several meters across and up to 1 m high in depths of about 4 m (Logan et al. 1974; Playford, 1990). These structures are weakly to poorly laminated, with coarse, irregular fenestrae and irregular outer surfaces (Playford 1990). Colloform mats have been variously described as gelatinous to leathery, pale yellowish-brown to gray, 1-2 mm thick with hollow contiguous convexities, 1-3 cm in diameter (Logan et al 1974) and as soft mats that are coherent at the surface, with lithification a few mm below the surface (Playford 1990). The mats are ephemeral, being widely established at times and absent at others (Logan et al. 1974).

The microbial community of the colloform mats is diverse and includes numerous prokaryotic and eukaryotic species. Logan et al. (1974) reported gelatinous mats dominated by filamentous *Microcoleus tenerrimus* and *Symploca laete-viridis* and thin leathery mats dominated by *Schizothrix helva*. Golubic (1992) described gelatinous colloform mats dominated by a coccoid entophysalidecean cyanobacterium that is new to science, with precipitation of tiny hollow aragonite spheres within these mats (Golubic 1992). Bauld reported a diverse diatom flora, whose role in mat construction is at least as import as cyanobacteria (reported in Playford 1990). Colloform mats are typically associated with the green algae *Acetabularia* sp. and ephemeral populations of encrusting foraminifers, molluscs, and serpulids.

Major factors in the growth of colloform mat stromatolites are reported as (1) doming of mats, (2) binding of sand, (3) precipitation and hardening of cryptocrystalline aragonite, and (4) oxidation of organic material (Logan et al. 1974). Lithified layers, 1-3 mm thick and composed of cryptocrystalline aragonite and variable quantities of peloidal grains and skeletal fragments, mimic domal undulations in the mat; these layers arch over elongate fenestrae, which tend to be elongated following the mat surface. The laminae are broken by *Acetabularia* holdfasts, which form cross cutting voids. Fenestrae may be open or infilled by detrital carbonate sediment (Logan et al. 1974).

Some stromatolite structures are reported to show a progression from one mat type to another. As subtidal stromatolites grow upward into the shallow subtidal or intertidal range, colloform mats may be replaced by smooth mats. Similarly, as lower intertidal stromatolites grow upward into the upper intertidal ranges, smooth mats may be replaced by pustular mats. Fenestral fabrics, which are characteristic of all the stromatolite types, are thought to be developed largely through decomposition of the enclosed mat material or by microbial mats bridging indentations on the stromatolite surfaces (Golubic 1983).

The growth history of stromatolites in Hamelin Pool is controversial. The structures were originally envisaged as primarily intertidal phenomena (Logan 1961; Logan et al. 1964). Subsequently, subtidal forms, with even more extensive distribution than the intertidal forms, were recognized (Playford and Cockbain 1976, Playford 1979, Walter and Bauld 1986). Playford (1990) argued that many of existing intertidal stromatolites have grown wholly in the intertidal

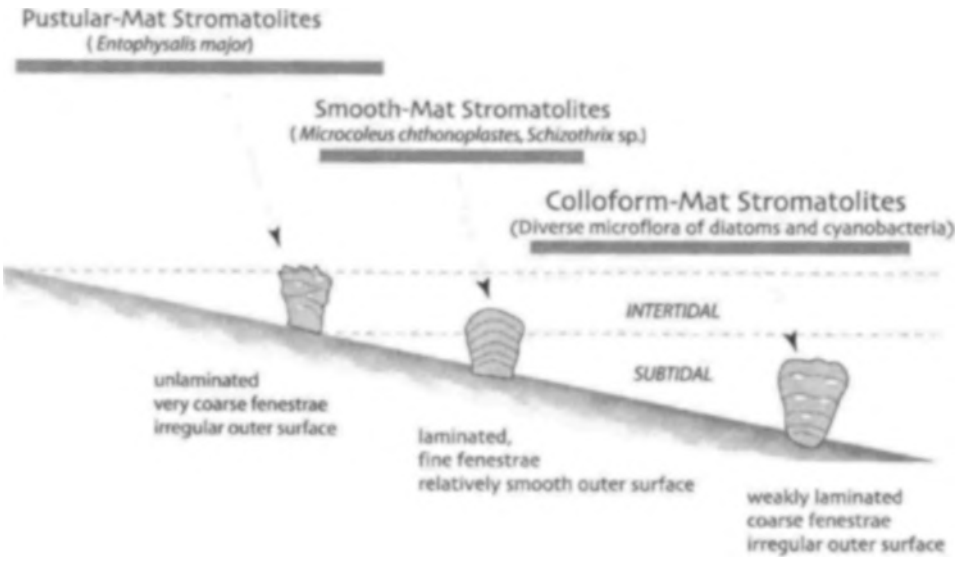

Fig. 2. Stromatolite distribution in Hamelin Pool as summarized by Playford (1990).

zone; others have suggested that present-day intertidal forms originated as subtidal stromatolites, which were veneered with intertidal growth as sea level fell (Burne and James 1986; Burne and Hunt 1990; Burne 1992

Radiocarbon dates by Chivas et al. (1990) indicate the following ages: a supratidal stromatolite was dated at 1250 –1010 years BP; one mid intertidal stromatolite was dated at 540-170 yrs BP, and another ranged from 930 yrs BP at the base to 520 yrs BP at the top; two subtidal stromatolites gave ages of 550-470 yrs BP at the base and 70-modern yrs BP at the top. These results suggest that subtidal stromatolite growth is presently active but that intertidal growth involves both past and modern accretion. Estimates of growth rates based on the radiocarbon dates suggest long-term vertical accretion is ≤ 0.4 mm/year. Thus individual stromatolites are estimated to have taken about 1000 years to reach their present growth heights of ~350 mm.

3 MATERIALS AND METHODS

Samples were collected from intertidal and subtidal environments at Carbla Point and Flagpole Landing, Hamelin Pool (Fig. 1, Pl. 45, Table 1). Most samples were collected during a Bureau of Mineral Resources, Baas Becking Laboratory expedition to Shark Bay in November 1985. The stromatolites were studied *in situ* and representative examples were sampled and returned to Canberra for analysis. These stromatolites were slabbed, and one half was impregnated with epoxy resin and saved as an archive specimen (Pl. 45/1d). A suite of thin sections was made from the other half, with 7-15 thin sections (2.5 cm x 4.5 cm) per stromatolite. Eight stromatolites and corresponding thin sections from the Baas Becking collection were analyzed for this study (Table 1).

The 1985 sample set was augmented by four smaller stromatolite samples collected by R.N. Ginsburg in 1979 and R.P. Reid in 1999. These stromatolites were slabbed and impregnated with epoxy; 1-3 large thin sections (5 cm x 7 cm) were made for each stromatolite. In addition to the primary set of 12 stromatolites (Table 1), we examined thin sections from from two additional samples in the mid intertidal zone (SB-99-4 and SB-99-8). SB-99-4 is a piece of pustular mat with a distinct knobby morphology (Pl. 45/1b); this characteristic mat type is referred to in this paper as knobby pustular mat.

Microfabrics were described by systematic mapping and photography of slabs and thin sections using binocular and petrographic microscopes. Selected thin sections were chosen for analysis using a scanning electron microscope (Philips XL-30 field emission SEM) equipped with Oxford Link energy-dispersive spectrometer (EDS) for elemental analysis. Sections were etched in 1% HCl for 5-10 seconds and lightly sputter coated (~ 10 nm) with palladium prior to SEM analysis.

Mineralogy was determined using a combination of light microscopy of petrographic thin sections, EDS analysis of SEM samples, and x-ray diffraction (XRD) of bulk samples Calcium carbonate with 1-2% strontium, as determined by EDS, was assumed to be aragonite. Aragonite in bulk samples was verified by XRD using a Scintag diffractometer with Cu Ka radiation over the range 25°-35° 2θ at a scan rate of 1°/min.

4 MICROFABRICS

In contrast to previous studies, which emphasized the sandy nature of Shark Bay stromatolites, we recognize two distinct microfabrics: grainy (or sandy), here called calcarenite, and muddy, here called micrite. The calcarenite and micritic groupings are further subdivided based on the presence or absence of lamination. In addition, a distinct micritic microfabric that forms a massive knobby caprock at the tops of some stromatolites is classified separately as Massive Micrite. An additional microfabric that is transitional between the calcarenite and micrite end members is also recognized. Characteristic features of each microfabric are described below; colors refer to appearance in plane-polarized light.

4.1 Calcarenite

Carbonate sand grains are the dominant component of this microfabric, forming grainstone, packstone, and, less commonly wackestone, textures. The sand is typically well sorted, ranging in size from 100-200 μm. Peloids (microcrystalline grains of unknown origin), foraminifera, shell fragments, and grains with superficial oolitic coatings are the major grain types; oolitic nuclei are mainly shell fragments and peloids. Larger foraminifera and bivalve shells up to several mm long are locally abundant, mainly in cavities. In addition to carbonate, quartz and dolomite typically comprise 5-10% of the grains and commonly form ooid nuclei. In some samples, the calcarenite is laminated; in other samples, it forms a heterogeneous, unlaminated fabric, as follows:

4.1.1 Laminated Calcarenite (LC, Pl. 46 and 47)

Description: Millimeter-scale lamination is defined by couplets of cemented and uncemented sand layers. The cemented laminae, typically 0.5-2 mm thick, appear as dense white bands in hand samples (Pl. 46/1a, Pl. 47/1a), and dark brown or gray bands in thin section, plane polarized light (Pl. 46/1b, 1c; Pl. 47/1b, 1c). Laminae are often convex upwards to wavy, and are laterally continuous for distances of several centimeters; in some cases, adjacent cemented horizons merge into a single band. Lamination is often enhanced by laminoid fenestrae or aligned pores. Elongate sand grains are also commonly aligned parallel to bedding. Two types of laminated calcarenite are recognized based on characteristic features of the cemented layers.

(a) Type 1 (LC-1, Pl. 46): LC-1 is the dominant form of laminated calcarenite. The characteristic feature of this microfabric is the presence of dark micritic coatings on carbonate sand grains in the cemented layers. These micritic coatings commonly have micropeloidal textures (peloids ~20 μm in diameter) and encompass silt-sized patches of translucent golden micrite (Pl. 46/1d-1f). The micritic coatings are in turn fringed with aragonite needle cement (Pl. 46/1f). In some cases, cemented laminae show an upward gradation from wackestone consisting predominantly of golden micrite with a granular texture to packstone or grainstone of micrite-coated sand grains (Pl. 46/1e). Layer thickness is irregular and varies between and within layers, generally ranging from 200 μm - 2 mm, but up to 5 mm thick.

Sand grains in LC-1 are typically fresh, with well preserved internal structure (Pl. 46/1d-f). In some cemented layers, however, grains are extensively altered, or micritized. The altered grains appear as peloids with a uniform grey appearance in plane polarized light, showing no internal structure (Pl. 46/1g); altered grains are commonly 'fused' or 'welded together' at point contacts (Pl. 46/1h). As in cemented layers of freshly preserved grains, the micritized grains are surrounded by dark micritic coatings with embedded golden granules and fringing aragonite needle cement (Pl. 46/1g, 1h). Some cemented layers show an upward gradation from fresh grains to micritized grains (Pl. 46/1g). Upper surfaces of the micritized horizons are typically abrupt and in some cases are defined by red-brown micritic crusts, also rimmed with dark micritic coatings (Pl. 46/1g).

Fenestrae (unsupported voids) are common in LC-1. Small irregular holes (< 1 cm) are abundant in cemented and uncemented layers and may be aligned along a layer (Pl. 46/1b). Elongate fenestrae, 1-2 cm long, are common, particularly in the cemented bands; poorly sorted geopetal sand, with large foraminifera and bivalve shells, often partially fills these cavities. Some larger cavities (1-4 cm) containing poorly sorted coarse-grained sand cut across the lamination. Truncated grains can be found at the margins of all cavity types, although many of the small pores and fenestrae exhibit no truncation.

(b) Type 2 (LC-2, Pl. 47): The second, and less common, laminated calcarenite microfabric, LC-2, is differentiated from LC-1 by a lack of dark micritic coatings and aragonite needle cement on sand grains in the cemented layers of the lithified/unlithified couplets. Cemented layers in LC-2 consist of horizons of extensively micritized grains. The micritized grains appear as structureless grey peloids that are fused together at point contacts (Pl. 47/1a-d). These layers of grey, welded grains form well-cemented layers 200-500 μm thick. Dolomite and quartz within these bands appear white in thin section, and stand out in sharp contrast to the surrounding micritized, gray grains (Pl. 47/1d). The upper boundaries of the micritized horizons are abrupt (Pl. 47/1d), and are commonly defined by micritic crusts, 20-50 μm thick (Pl. 47/1e). Upper surfaces of micritized grains below the micritic crusts are often truncated (Pl. 47/1f). Fenestrae and other small cavities are common in LC-2, and are often aligned with a single layer. Particles at the margins of these cavities are generally not truncated

SEM photomicrographs show that micritized horizons in both LC-2 and LC-1 form as a result of microboring. In LC-2, micritized grains are permeated by bore holes that are infilled with micritic cement (Pl. 48/1b). The bore holes are approximately 10 μm in diameter; they form elongate tracks, which follow grain outlines, leaving the margins of the grains intact (Pl. 48/1d). Infilling consists of needle-shaped aragonite crystals that form scalloped patterns perpendicular to the direction of boring (Pl. 48/1d,1e). Infilling of bore holes that cross between grains at point contacts (Pl. 48/1c) results in grain fusion. Advanced fusion leads to obliteration of original grain outlines. The aragonite crystals in the bore holes are about 0.5 microns wide and 2 μm wide. The crystals have a characteristic granular structure, being composed of tiny crystallites about 50 nm in size (Pl. 48/1f).

Micritized horizons in LC-1 (Pl. 48/2) show microboring features similar to those in LC-2. Micritized grains are permeated with infilled bore holes and grains are fused as result of microboring tracks crossing between grains at point contacts. The micropeloidal coatings and fringing aragonite needle cements, which characterize LC-1 but are absent in LC-2, are not microbored (Pl. 48/2b).

Distribution: Laminated calcarenite is restricted to the intertidal zone (Fig. 3). LC-1 is the dominant microfabric of the

Tidal zone Sample #	Collection site	Date collected	Sample height	Field description of surface mat	Tidal zone or depth; additional comments
Intertidal					
866	Carbla	1985	26 cm	film	supra to upper intertidal; buried except for top, which sticks out of sand
867	Carbla	1985	41 cm	film	upper to mid intertidal
842	Flagpole Landing	1985	40 cm	knobby pustular	mid intertidal
841	Flagpole Landing	1985	43 cm	pustular	lower intertidal; grey base in sediment
SB-99-1	Carbla	1999	14 cm	pustular	lower intertidal
79-136	Carbla	1979	20 cm	pustular	lower intertidal
SB-99-5	Carbla	1999	8 cm	smooth	lower intertidal to shallow subtidal
Subtidal					
858	Carbla	1985	26 cm	no mat	1 m depth; thin surface mat observed in thin section
79-135.4	Carbla	1979	13 cm	no mat	depth unknown
844	Carbla	1985	19 cm	no mat	1 m depth
857	Carbla	1985	24 cm	no mat	1.5 m depth; thin surface mat observed in thin section
843	Flagpole Landing	1985	33 cm	no mat	2 m depth

Table 1. Samples analyzed for the present study; depth refers to height of water above top of stromatolite at time of collection.

large stromatolite heads 866 and 867, from the upper intertidal zone, and in the smaller stromatolite 79-136 from the lower intertidal zone. Field descriptions at the time of collection (Table 1) classified surface mats on these stromatolites as film (866, 867) and pustular (79-136). LC-2 microfabric is the dominant component of small, topographically low stromatolites (e.g. SB-99-5), which occur in the lower intertidal to shallow subtidal zone between the larger stromatolites. These stromatolites are colonized by smooth mats. LC-2 also forms the base of mid intertidal stromatolite SB-99-1.

Origin: Laminated calcarenite is interpreted as a primary depositional microfabric, with couplets of cemented and uncemented sand representing discrete accretionary events. Fenestrae in the laminated calcarenite could represent buckling of a microbial mat due to air bubbles (Monty 1976), degradation of a mat, holdfasts, or holes from boring organisms. Truncated grains at cavity margins indicate that at least some of the holes are diagenetic products resulting from boring activities.

Insight into the role of organisms in the formation of laminated calcarenite comes from comparison with Bahamian stromatolites Exuma stromatolites (Lee Stocking Is.) exhibit many features that are identical to those observed in LC-2. Indeed, except for the presence of minor amounts of quartz and dolomite in LC-2, which are lacking in the Bahamian structures, Pls. 3/1 and 4/1 could be photomicrographs of Exuma stromatolites. The succession of couplets of well preserved, well sorted, uncemented sand alternating with cemented bands of grey micritized fused grains capped with micritic crusts in LC-2 (Pl. 47/1) is identical to the pattern in Exuma stromatolites. In addition, the dimensions and patterns of the infilled bore holes, within and crossing between grains, in the grey micritized horizons (Pl. 48/1) are identical to the microboring patterns observed in the micritized horizons of Exuma stromatolites (Macintyre et al. 2000).

Previous work has shown that lamination in Exuma stromatolites results from a cycling of surface microbial communities (Reid et al 2000). The binding and trapping of well sorted, fine grained sand by the filamentous cyanobacterium, *Schizothrix* sp., forms unlithified grain layers. During a hiatus in sedimentation, a surface biofilm develops, with abundant heterotrophic bacteria. Thin micritic crusts (20-50 µm) precipitate in the biofilm as a result of heterotrophic activity (Visscher et al. 1998, 2000). During longer periods of hiatus, the coccoid endolithic cyanobacterium *Solentia* sp. infests carbonate grains below the biofilm. Carbonate precipitation within an organic gel matrix in the bore holes concurrent with endolithic activity welds grains together, forming cemented horizons of fused, micritized grains (Macintyre et al. 2000). A characteristic feature of sand accreted by *Schizothrix* is the absence of

Plate 45 Hamelin Pool stromatolites (Western Australia).

Fig. 1a. Field photographs at Carbla Point showing upper to mid intertidal stromatolites with pustular surface mats; stromatolites are approximately 40 cm high.

Fig. 1b. Mid to lower intertidal stromatolites at Carbla Point with knobby pustular (k), pustular (p) and smooth (s) surface mats; film mat (f) caps the tallest stromatolite (~0.5 m), which extends into the upper intertidal zone.

Fig. 1c. Subtidal stromatolites, 20-50 cm high, approximately 1 m water depth, Carbla Point; upper surfaces are coated with loosely bound sediment that has been referred to as colloform mat; sides are colonized by *Acetabularia*.

Fig. 1d. Vertical sections through slabbed field specimens; 866, supra to upper intertidal; 842, mid intertidal; 79-136, lower intertidal; SB-99-5, lower intertidal; 857, subtidal zone.


1a

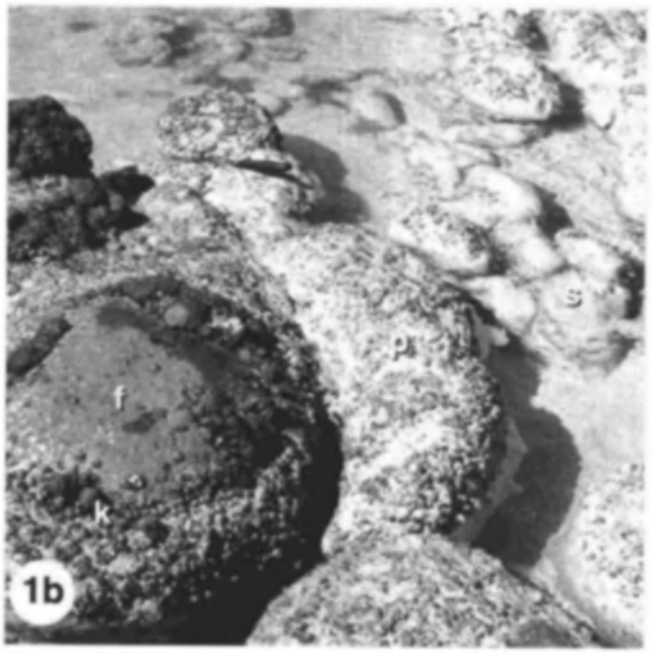
s
p
f
k
1b

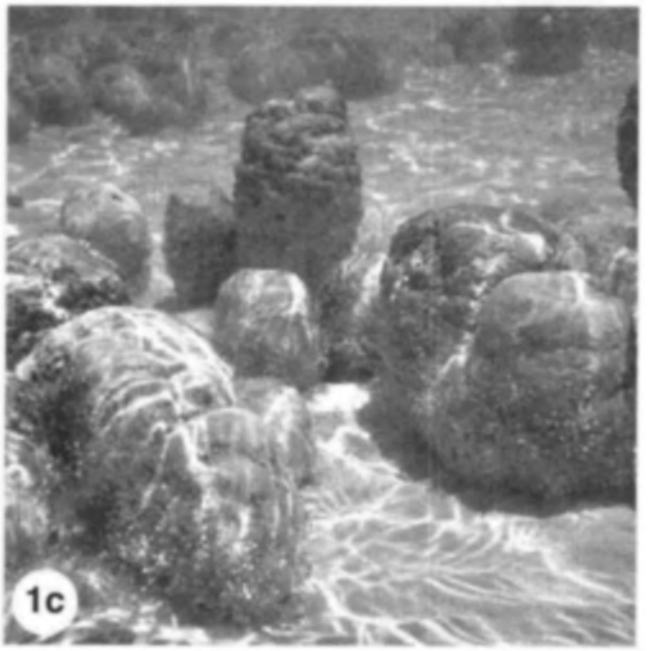
1c

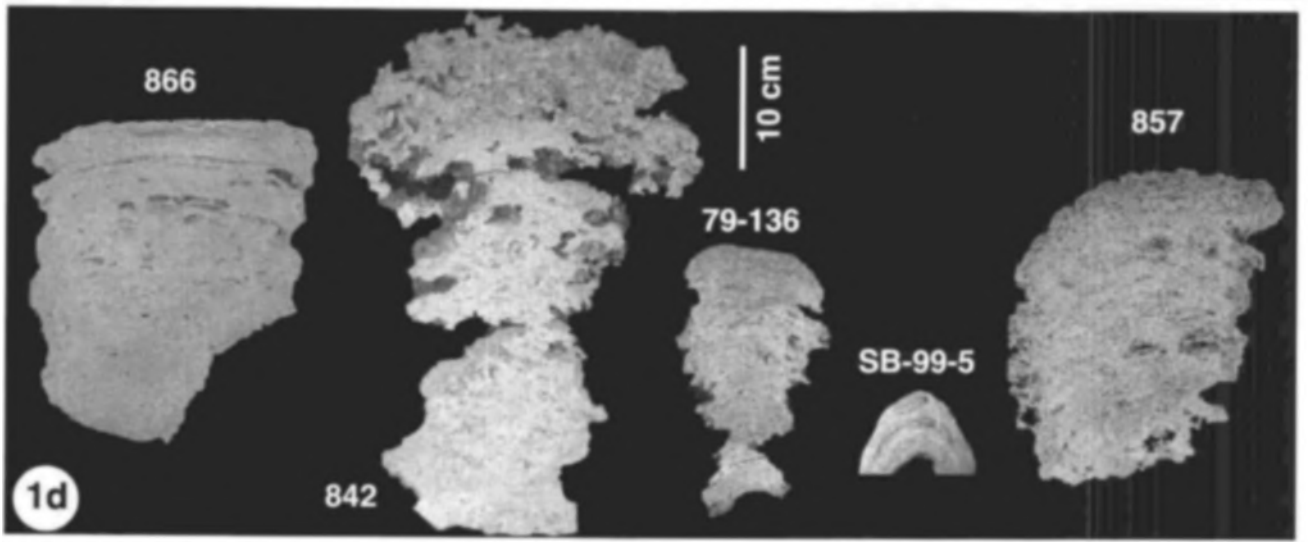
866
10 cm
857
79-136
SB-99-5
842
1d

interstitial submarine fringe cement, because pore-filling polymeric secretions of *Schizothrix* inhibit precipitation (Kawaguchi and Decho 2002).

The similarities in microfabrics of LC-2 and Exuma stromatolites suggest that lamination in LC-2 results from a cycling of surface communities similar to that documented in the Bahamian examples. Thus the uncemented grain layers in LC-2 are interpreted to accrete through the binding and trapping activities of *Schizothrix* or similar filamentous cyanobacteria such as *Microcoleus*. The micritic crusts of LC-2 (e.g. Pl. 47/1e) are interpreted to precipitate within bacterial biofilms formed during short hiatuses in sedimentation. Micritized horizons (e.g. Pl. 47/1d) develop during longer hiatal periods, when grains become infested with the endolithic cyanobacterium *Solentia* sp.; carbonate cemented precipitated in bore holes crossing between grains welds them together (Pl. 48/1b, 1c). This interpretation is consistent with the presence of smooth mats, which previous authors reported are dominated by *Schizothrix* or *Microcoleus* (e.g. Logan et al 1974, Golubic 1985), on the surfaces of lower intertidal and shallow subtidal stromatolites comprised mainly of LC-2 (e.g. SB-99-5, Fig. 3, Table 1).

In contrast to LC-2, features in LC-1 are distinctly different from those in Exuma stromatolites. In particular, cemented layers with micritic coatings on sand grains and aragonite needle cement are lacking in Exuma stromatolites. Indeed, as noted previously, syndepositional precipitation in interstitial spaces between grains accreted by *Schizothrix* is inhibited by *Schizothrix* polymers (Kawaguchi and Decho 2002). Thus, the cemented layers of LC-1 did not form in *Schizothrix* mats.

So what is the origin of LC-1, the dominant microfabric of laminated stromatolites in the intertidal zone? Our interpretation is limited by a lack of detailed microbiological studies. The dark micropeloidal coatings with enclosed patches of golden precipitate and fringing aragonite needle cement (Pl. 46/1d, 1f) suggest, however, that cementation occurred in mats dominated by *Entophysalis major*. Micropeloidal texture is a characteristic feature of micrite precipitated in microbial mucous or organic gel (Dupraz and Strasser, 1999, 2002; Reitner, 1993; Riding, 1991, 2000). In addition, precipitates formed by lithification of *E. major* have a characteristic golden to red-brown color and these biological precipitates are typically coated with abiotic aragonite fringe cement (Golubic 1985, 1992). Finally, dark micritic coatings, golden micritic granules, and fringing aragonite needle cement are characteristic features of the massive micrite fabric, described in Ch. 4.2.1, which is a product of *E. major* lithification. We therefore interpret that sand in the cemented layers of LC-1 was trapped and bound by soft *Entophysalis* mats and subsequently cemented during episodic mat calcification. The flat upper surfaces of the cemented layers (e.g. Pl. 46/1d) indicate that the *Entophysalis* mats in which they formed were relatively smooth.

The micritized horizons that characterize some cemented layers in LC-1 (e.g. Pl. 46/1g, 1h) are thought to represent periods of *Solentia* infestation of grains trapped by *Entophysalis* prior to mat lithification. This is based on the

Plate 46 Hamelin Pool stromatolites (Western Australia). Laminated Calcarenite Type 1 (LC-1) microfabric. Unless otherwise indicated, figures in all plates are thin sections photographed using a petrographic microscope with plane-polarized light; color descriptions refer to observations in plane-polarized light.

Fig. 1a. Vertical section through a slabbed field specimen with laminated structure defined by dense, white bands. Fenestrae of variable shapes and sizes are common; some are elongate parallel to lamination. Sample 867.

Fig. 1b. Low magnification photomicrograph showing a distinct banded pattern, emphasized by an alignment of pores. Thin section SB-99-1-B.

Fig. 1c. Higher magnification view showing alternating layers of loose and cemented sand; the cemented layers (arrows), which appear dark in thin section, are the white bands of Fig. 1a. Thin section SB-99-9A.

Fig. 1d. Detailed view of cemented layer with abrupt upper surface (arrow), showing well preserved oolitic sand grains embedded in golden brown micrite; sand grains above and below this cemented layer lack conspicuous pore filling. Thin section SB-99-8.

Fig. 1e. Cemented layer that grades upward from a wackestone of grains floating in golden micrite (m) to a packstone or grainstone of oolitic grains with micritic coatings and aragonite needle cement. Thin section 867-D.

Fig. 1f. Detailed view of cemented layer showing fresh sand grains, with well preserved internal structure, rimmed by dark micritic coatings (d) with embedded golden granules (gr); aragonite needle cement (an) is infilling remaining pore space. Thin section SB-99-1-A.

Fig. 1g. Cemented layer showing upward gradation from fresh grains (fg) to grey micritized grains (mg); both fresh and altered grains are rimmed with dark micritic coatings. The sharp upper boundary of the micritized horizon is defined by a micritic crust (arrow); the crust has a red brown color and is also rimmed with dark micrite. Thin section SB-99-1-B.

Fig. 1h. Higher magnification view of a micritized horizon showing fusion of grains at point contacts (arrows); quartz (q) and dolomite (d) grains are not microbored. Micritized grains are coated with dark micropeloidal micrite (arrow, peloids ~ 20 μm), in turn coated with aragonite needle cement. Thin section 866-C1.

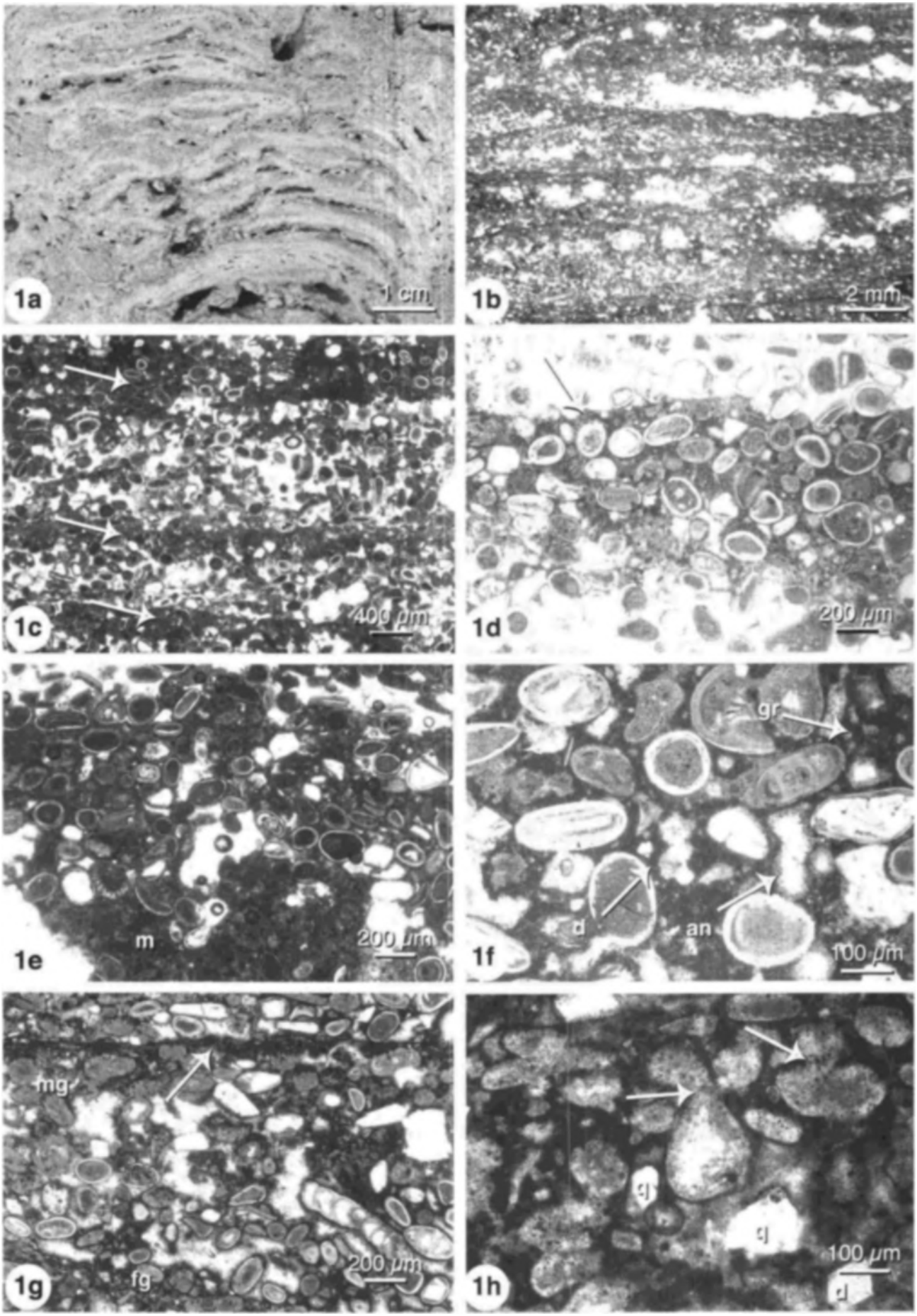
1a
1 cm
1b
2 mm
1c
400 µm
1d
200 µm
1e
m
200 µm
1f
gr
d
an
100 µm
1g
mg
fg
200 µm
1h
gl
gl
100 µm
gl

similarity of microboring patterns and infilling cements in these grains (Pl. 48/2a,2b) to micritized grains in LC-2 (Pl. 48/1a-1f). In the case of LC-1, micritized grains were subsequently encased by micritic coatings and fringe cement, which were not microbored (Pl. 48/2a, 2b), during episodic lithification of *Entophysalis*.

Uncemented layers in LC-1could have accreted through trapping and binding by *Entophysalis* mats during periods of non lithification, or through binding and trapping by smooth mats dominated by filamentous cyanobacteria such as *Schizothrix* or *Microcoleus*. The sand, which is well sorted and fine grained, is texturally similar to sand in Exuma stromatolites that is accreted by *Schizothrix*. Couplets of cemented-uncemented layers in LC-1 could, therefore, represent a cycling of surface microbial communities between *Entophysalis*-dominated mats and *Schizothrix*-dominated smooth mats, with cementation resulting from calcification of *Entophysalis*. A shift from coccoid to filamentous cyanobacteria could occur in response to sedimentation or burial.

The distribution of LC-1 as the dominant component of stromatolites in the upper intertidal zone (866 and 867, Fig. 3) and some stromatolites in the lower intertidal zone (79-136, Fig. 3) is noteworthy. Stromatolites 866 and 867 were colonized primarily by black film mat at the time of collection. Film mat was described by Logan et al. (1974) as a desiccated ecomorph of *Entophysalis*, and by Golubic (1983) as consisting of *Hormathonema* endoliths. Previous authors (e.g. Playford and Cockbain 1976, Playford 1990) have suggested that desiccated stromatolites above the high-tide level are dead. In contrast, the lower intertidal zone, where stromatolite 79-136 was collected, is colonized by actively growing smooth and pustular mats (Pl. 45/1b), and alternation between these mat types is a likely origin of the LC-1 microfabric. Thus LC-1 stromatolites that are presently in the upper intertidal zone are interpreted to be inactive, relict structures, which formed in lower intertidal zones when sea level was higher.

4.1.2 Unlaminated Calcarenite (UC, Pl. 49)

Unlaminated calcarenite is a heterogeneous sandy microfabric; couplets of cemented-uncemented layers are not present. Slabbed field samples show a mottled network of dense white limestone and irregular fenestrae (Pl. 49/1a). Low magnification views of thin sections show a disorganized pattern of limestone and fenestrae (Pl. 49/1b). Fenestrae, which are equidimensional to elongate and typically 1-3 mm in size, occupy ~20% of the bulk volume. Larger, cm-scale vugs that are commonly filled with chalky sediment are also present.

Examination with a petrographic microscope indicates that this microfabric is characterized by the same cemented textures present in LC-1. These textures, however, are arranged in patchy, rather than banded, patterns (Pl. 49/1c, d). Fresh sand grains rimmed by dark crusts of micropeloidal micrite in turn coated by acicular aragonite form grainstone patches; well preserved sand grains are also found floating in golden mottled microcrystalline matrix, forming wackestones. Patches of dark micrite with golden granule inclusions (Pl. 49/1d), golden granular micrite (Pl. 49/1e) and sand grains rimmed with dark micrite (Pl. 49/1f) are common. Areas of grey micritized grains or clotted micrite lacking distinct grain outlines (Pl. 49/1f, 1g) are also prevalent; occasional skeletal grains within these grey areas are typically micritized and losing definition.

Many small fenestrae in the mottled calcarenite are filled with aragonite needle cement (Pl. 49/1c). Margins of open fenestrae and cm-scale vugs commonly show truncated grains (Pl. 49/1h). Some large cavities are partially filled with poorly sorted, coarse-grained sediment, including large

Plate 47 Hamelin Pool stromatolites (Western Australia).

Part 1 Laminated Calcarenite Type 2 (LC-2) microfabric.

Fig. 1a. Vertical section through a slabbed field specimen showing layered structure defined by dense white bands. Sample SB-99-5.

Fig. 1b. Low magnification photomicrograph showing couplets of cemented and uncemented sand; the cemented layers (arrows), which appear grey in plane-polarized light, are the white bands of Fig. 1a. Thin section SB-99-5.

Fig. 1c. Higher magnification view showing several micritized horizons composed of grey structureless grains that are fusing together. Detail of white boxed area is shown in Fig. 1d; SEM view of area in dashed black box is shown in Pl. 48/1a. Thin section SB-99-1B.

Fig. 1d. Detail of micritized horizon indicated in Fig. 1c. Peloidal grains are extensively fused so that grain outlines are barely visible. Dolomite (d) and quartz (q) appear white, in sharp contrast to the grey fused peloids. Thin section SB-99-1B

Fig. 1e. Micritic crust (arrow) overlying grey micritized grains. Thin section SB-99-3b.

Fig. 1f. Micritized grains with truncated upper surfaces (arrows) below the micritic crust. Thin section SB-99-5.

Part 2 Micrite-Calcarenite (M-C) transitional microfabric.

Fig. 2a. Early stage: Initial infilling of pore space between micritic bands with calcarenite. Sand grains are coated with dark, micropeloidal micrite and aragonite needle cement. Thin section 858-E

Fig. 2b. Late stage: Complete infilling of pore space between micritic bands with calcarenite. Sand grains in a matrix of dark micropeloidal micrite fill pore space between micritic bands. The original structure of laminated micrite is almost lost and the fabric is gradational to unlaminated calcarenite. Thin section 841-E.

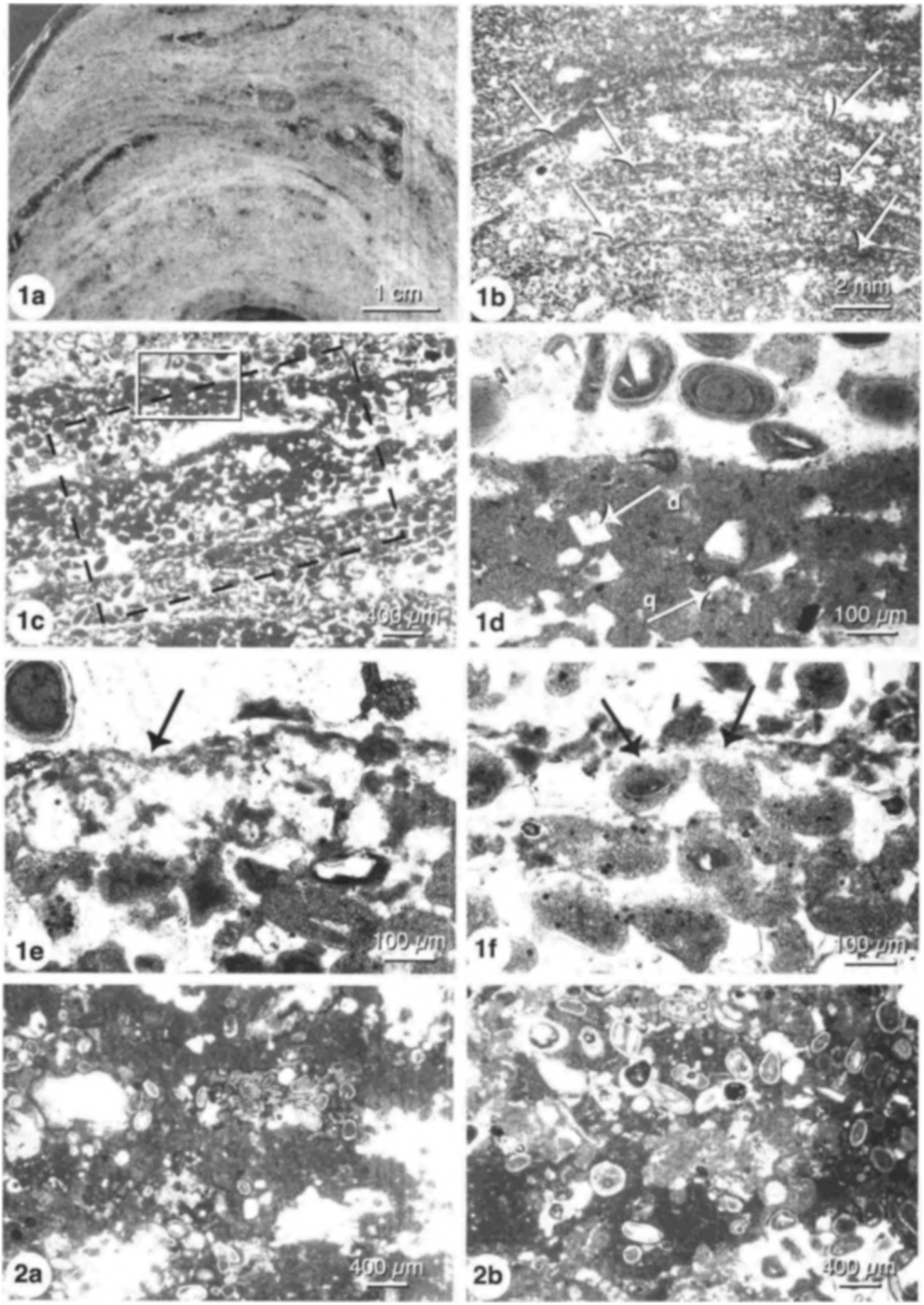
1a
1 cm
1b
2 mm
1c
400 µm
1d
d
q
100 µm
1e
100 µm
1f
100 µm
2a
400 µm
2b
400 µm

foraminifera (1-2 mm) and bivalves (3-5 mm); cavity-filling internal sediments often have a golden to red brown micritic matrix (Pl. 49/1g).

Distribution: Unlaminated calcarenite is the dominant microfabric in stromatolites 842 and 841 in the mid to lower intertidal zone (Fig. 3). This fabric also forms the base of subtidal stromatolites 857 and 843 (Fig. 3).

Origin: Unlaminated calcarenite in the intertidal zone is interpreted as a primary depositional microfabric. Components comprising UC are basically the same as those in the cemented layers of LC-1: fresh grains rimmed with micropeloidal micrite and aragonite needle cement (Pl. 49/1d, 1f, 1h), golden granular micrite (Pl. 49/1e), and micritized grains (Pl. 49/1f). In UC, however, these components have patchy, rather than laminar distributions. UC is further differentiated from LC-1 by the lack of layers of uncemented sand. A probable explanation for such similarities and differences is that, in contrast to cement layers of LC-1, envisaged to form in flat ecomorphs of *Entophysalis* mat, UC formed in pustular *Entophysalis* mats with irregular, warty surfaces. The irregular surface morphology inhibits layer formation. The common occurrence of truncated grains at cavity margins is evidence for at least some post depositional boring and cavity formation.

An alternative interpretation is that UC is a reworked microfabric formed as a result of multicyclic boring and infilling of a preexisting stromatolite. This is a possible origin of UC at the base of subtidal stromatolites 857 and 843, where 2nd generation infilling of cavities with cemented sediment is a dominant petrographic feature (e.g. Pl. 49/1g).

4.2 Micrite

The micritic microfabrics are composed mainly of microcrystalline aragonite, which commonly displays a clotted texture. Three varieties of are recognized: massive micrite (MaM), laminated micrite (LM), and unlaminated micrite (UM), as described below.

4.2.1 Massive Micrite (MaM, Pl. 50)

Description: In slabbed hand specimens, the massive micrite microfabric appears as a dense, mottled mixture of greenish to light brown limestone (Pl. 50/1a). The surface morphology has a characteristic knobby appearance resulting from the growth of convex upwards accretionary surfaces (Pl. 50/1a). Bivalve fragments up to several millimeters in length are locally abundant (Pl. 50/1a). Voids space, including irregular pores, and circum convex and radial cracks comprise ~30% of the volume.

Thin section observations show a micritic framework with a second generation of infilling sediment (Pl. 50/1b). The micrite has a characteristic golden to red-brown color; XRD analyses of five bulk samples indicate that it is aragonite. Dense homogeneous micrite grades to more open equant clusters, 20-50 μm in size (Pl. 50/1c, 1d). Filament molds are sometimes present and small dark inclusions (10 μm) are locally abundant (Pl. 50/1e). Dense micrite may grade to micrite with a granular appearance; 'granules' are 20-100 μm in size, surrounded by dark rims and acicular aragonite cement (Pl. 50/1f).

Sand grains, including superficial ooids, foraminifera, and bivalves, with minor amounts of quartz and dolomite

Plate 48 Hamelin Pool stromatolites (Western Australia). Scanning electron photomicrographs of features observed in petrographic thin sections lightly etched in 1% HCl for 5-10 seconds and coated with palladium; sample SB-99-1b.

Part 1. Laminated calcarenite, Type 2 (LC-2)

Fig. 1a. Low magnification SEM photomicrograph of micritized horizons shown in boxed area of Pl. 47/1c. Box and arrow on this figure indicate locations of Pl. 48/1b, 1c.

Fig. 1b. Boxed area in Fig. 1a showing grains permeated with bore holes that are infilled with cement; note the fusion of grains, which results in loss of original grain outlines. Quartz grains (q) are not microbored.

Fig. 1c. Detailed view of point contact between two fused grains showing infilled bore hole that crosses from one grain to the other (arrow). Carbonate precipitation within the bore holes concurrent with endolithic activity welds grains together.

Fig. 1d. Typical pattern of bore hole infilling. Bands of aragonite needles are precipitated across the hole, forming a scalloped pattern. Note that the borehole follows the grain perimeter, but does not penetrate the grain margin.

Fig. 1e. Higher magnification view highlighting the banded nature of the elongate crystals that infill the boreholes. This infilling pattern is characteristic of the endolithic cyanobacterium, *Solentia* sp., which forms layers of fused micritized grains in Bahamian stromatolites.

Fig. 1f. Detailed view of the elongate crystals within the boreholes; the granular appearance is characteristic of *Solentia* infilling in Bahamian stromatolites.

Part 2. Laminated calcarenite, Type 1 (LC-1)

Fig. 2a. Low magnification view of a micritized horizon in an LC-1 microfabric similar to that shown in Pl. 46/1g; micritized grains are surrounded by dark micropeloidal coatings and fringe cement. Detail of boxed area is shown in Fig. 2b.

Fig. 2b. Detail of 2a. Note that the micritized grains (m) are permeated with infilled microborings. The micropeloidal coatings and fringe cement (arrow) surrounding the micritized grains are not microbored.

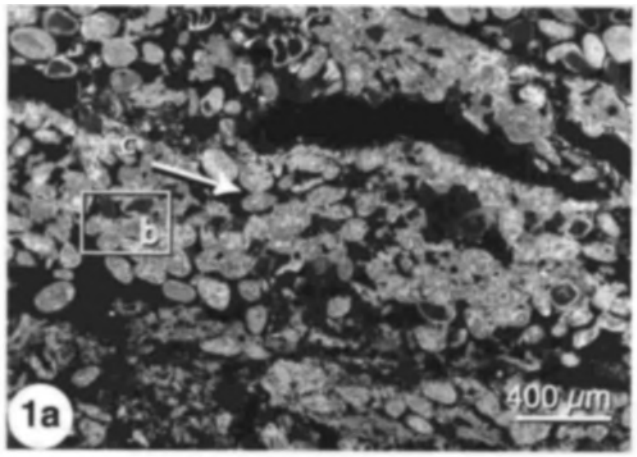
b
400 µm
1a

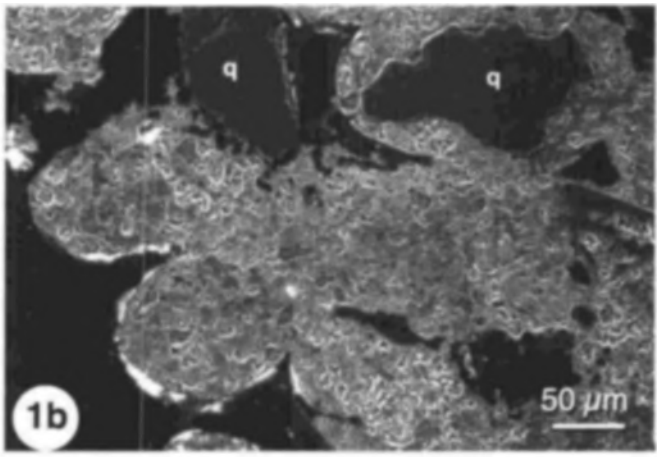
q
q
50 µm
1b

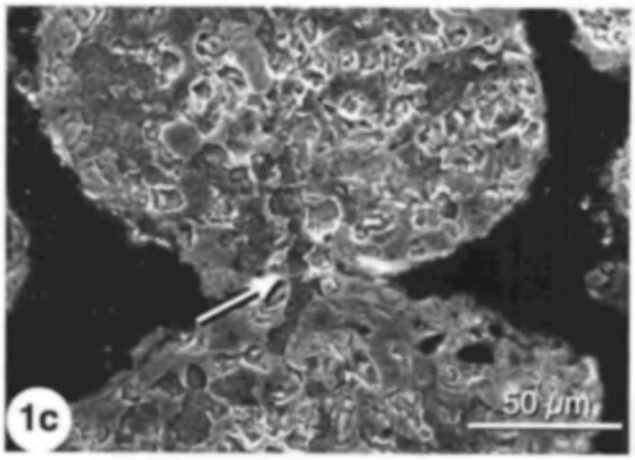
50 µm
1c

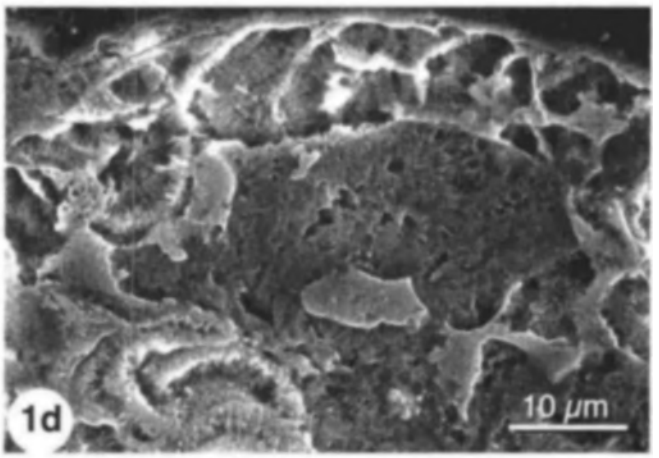
10 µm
1d

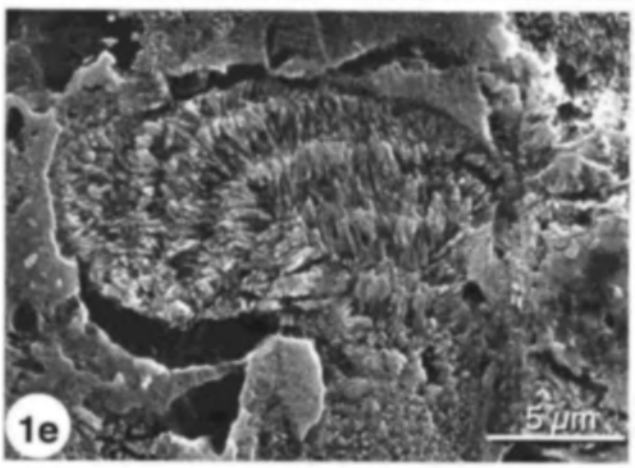
5 µm
1e

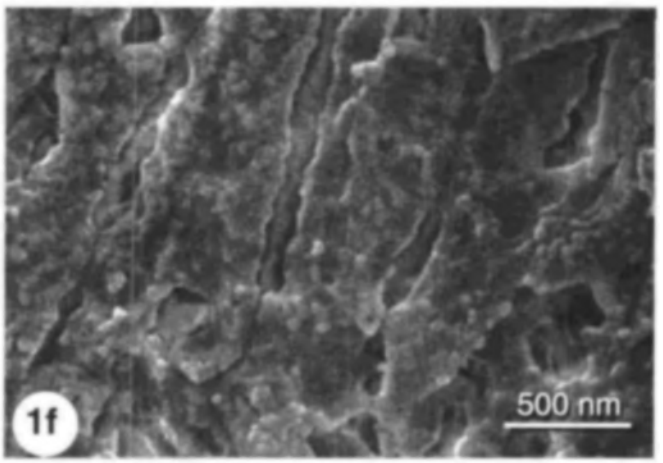
500 nm
1f

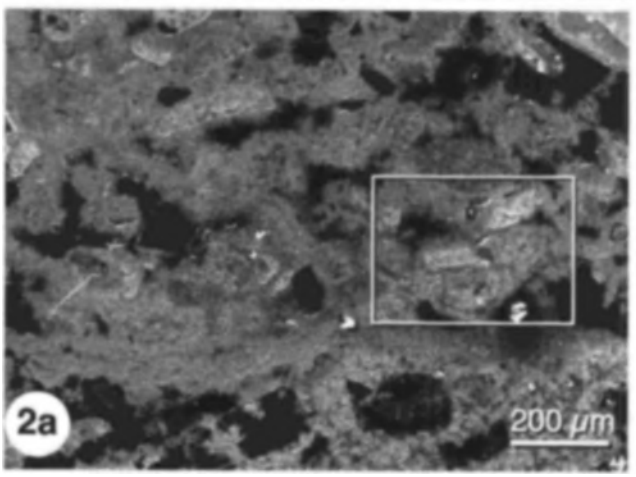
200 µm
2a

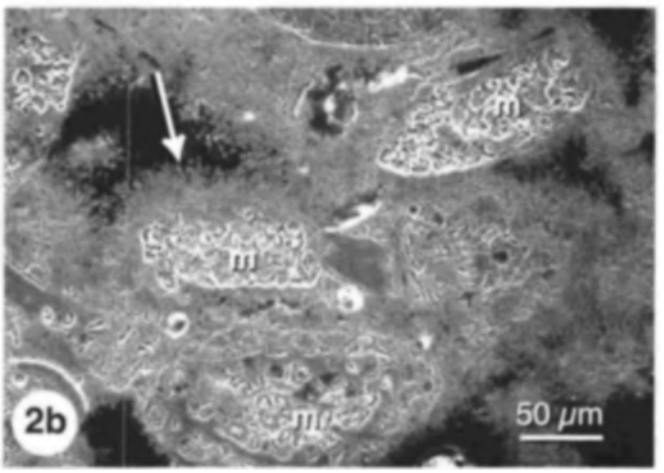
m
m
m
50 µm
2b

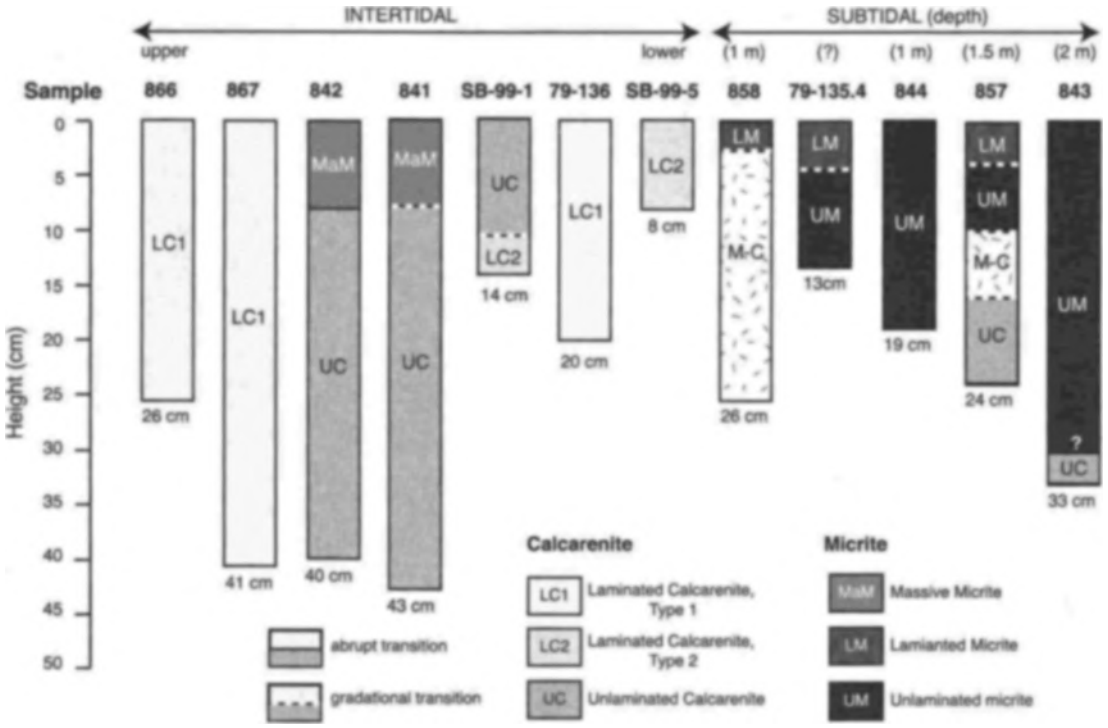

Fig. 3. Gross distribution of dominant microfabrics in samples analyzed for the present study. Depths in parentheses indicate height of water above the top of subtidal stromatolites at the time of collection; numbers at base of columns indicate stromatolite height.

may be scattered within the micrite but, more commonly, sediment occurs as cavity fillings (Pl. 50/1b, 1g, 1h, Pl. 51/1a). These cavity-filling sands appear as the light brown areas in the slabbed section (Pl. 50/1a). Red brown micrite, which may have a granular texture, commonly fills interstitial spaces within the cavities (Pl. 50/1g). Grains within the red-brown matrix show varying degrees of micritization: heavily micritized grains merge with the micritic matrix and become unrecognizable (Pl. 50/1h).

SEM observations show that crystal growth initiates within an organic matrix (Pl. 51/1a-1f). At the surface of the knobby projections, globular to ovoid crystals, 0.1-0.3 µm in diameter, are embedded in gel (Pl. 51/1b). About 2 mm below the surface, the gel is patchy and submicron-sized crystals have irregular to ovoid shapes (Pl. 51/1c). At several centimeters depth, elongate needle to rod shaped crystals, about 1 µm long and 0.1-0.3 µm wide, form a uniform texture with no apparent gel.

Distribution: Massive micrite forms knobby caps several centimeters thick, which overlie unlaminated calcarenite in stromatolites 842 and 841 (Fig. 3). The bases of 842 and 841 are in the lower intertidal zone, but they are >40 cm tall and their surfaces are in mid to upper intertidal zones; these surfaces are colonized by knobby pustular mats (Table 1, Pl. 1/1b). The transition from massive micrite to unlaminated calcarenite is abrupt in 842 and gradational in 841 (Fig. 3).

Plate 49 Hamelin Pool stromatolites (Western Australia). Unlaminated Calcarenite (UC) microfabric.

Fig. 1a. Vertical section through a slabbed field specimen showing the heterogeneous fabric consisting of a mottled network of dense limestone with small, irregular fenestrae. Sample 842.

Figs. 1b. Low magnification photomicrograph showing the heterogeneous fabric and irregular fenestrae. Note bivalve shells on lower left (arrows) and the truncated shell (t at the pore margin. Thin section 842-F.

Figs. 1c, 1d. Higher magnification views showing patchy distribution of grainstone (gn), packstone (p), and micrite (m); some of the small fenestrae in Fig. 1c are completely infilled with aragonite needle cement (an). Fig. 1c: thin section 842-F; Fig. 1d: thin section 842-L.

Fig. 1e. Golden micrite with a granular texture; golden granules (g) are rimmed by dark micrite and small cavities are infilled with aragonite needle cement (an).

Fig. 1f. Abrupt contact between grey clotted micrite (m) and patch of grainstone (gn) composed mainly of carbonate grains rimmed by dark micrite and fringe cement. Thin section 857-O.

Fig. 1g. Grey micrite (m) abuts a cavity partially infilled with large bivalve shells (s) and sand grains that are interconnected by a red brown micritic matrix (white arrow); small cavities are infilled with aragonite needle cement (an). Thin section 841-E.

Fig. 1h. Margin of fenestral cavity showing truncation of oolitic grains (arrows); the grains are coated with dark micrite, in turn coated with needle fringe cement. Thin section 842-G.

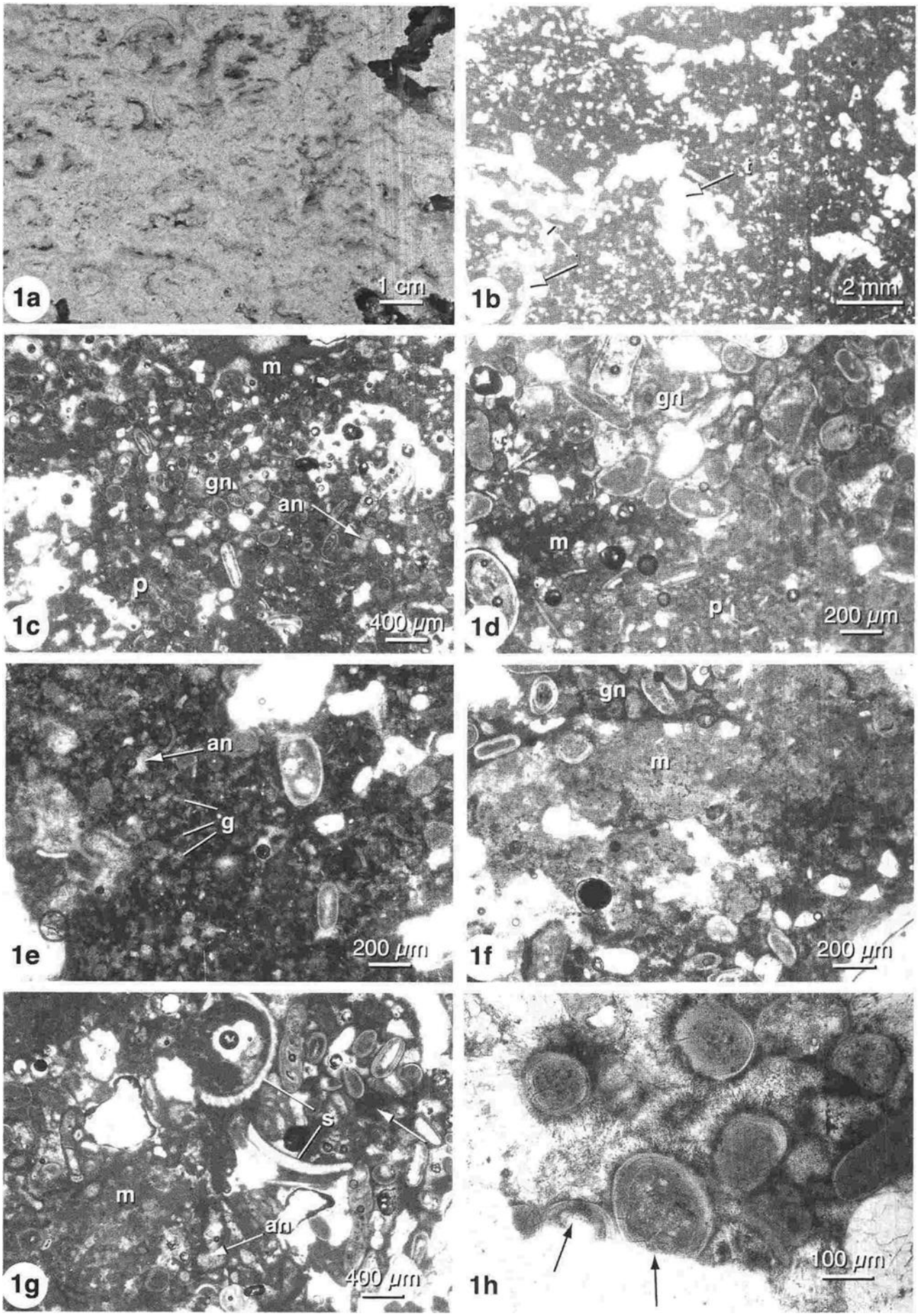
1a
1 cm
1b
A
t
2 mm
1c
m
gn
an
p
400 µm
1d
gn
m
p
200 µm
1e
an
g
200 µm
1f
gn
m
200 µm
1g
s
m
an
400 µm
1h
100 µm

Origin: Massive micrite is interpreted as a primary depositional microfabric, with infilling of original cracks with a second generation of internal sediment. This knobby microfabric, which caps mid-intertidal stromatolites composed mainly of UC (Fig. 3), represents calcified knobby *Entophysalis* mat (Pl. 45/1b) with little to no trapped and bound sediment. MaM has the characteristic red-brown to golden color (Pl. 50/1b-1g) of *Entophysalis* precipitates (Golubic 1983, 1992). The black inclusions (Pl. 50/1c) may be shriveled *Entophysalis* cells or bacteria entombed by the calcification process (cf. Golubic 1983). Intimate relationships between organic gel and precipitated crystals at the uppermost surface of the accreting knobs (Pl. 51/1b) is further evidence of a biologic origin. Precipitation of $CaCO_3$ within the pustular mats is reported to begin in polysaccharide envelopes surrounding *E.major* cells (Golubic 1983, 1992). Globular crystal shape, as observed in the initial precipitates (Pl. 51/1b), is typical of amorphous carbonate formed in biological systems (Golubic 1983). Progression from globular to irregular ovoid (Pl. 51/1c) and finally elongate, needle and rod-shaped crystals (Pl. 51/1d) may accompany the development of an organized aragonite crystal structure. Biologic precipitation of golden micrite within the *Entophysalis* mats is followed by abiotic precipitation of crusts of aragonite needle cement (Pl. 50/1f) as described by Golubic (1983, 1992).

Convex upward and radial cracks within the massive micrite (Pl. 50/1b, Pl. 51/1a) are interpreted to form as a result of desiccation of the pustular mat. Sediment that filters into these cracks forms geopetal infilling. The red-brown micritic matrix of the internal sediment (Pl. 50/1g, 1h) is likely formed by calcification of *Entophysalis* cells within these cavities. Micritization of skeletal grains within the cavities (Pl. 50/1h) may result from microboring by *Solentia*, as described by Reid and Macintyre (2000).

4.2.2 Laminated Micrite (LM, Pl. 52)

Millimeter scale lamination in the LM microfabric is defined by bands of open space alternating with bands of microcrystalline aragonite. This banding pattern is seen in slabbed hand specimens (Pl. 52/1a) and in low magnification thin section photomicrographs (Pl. 52/1b). The micritic bands are 200 µm to 2 mm wide and most are laterally continuous for distances of several centimeters. Pore spaces between the micritic bands also range from about 200 µm to 2 mm in height.

Higher magnification photomicrographs show progressive development of micritic bands with clotted texture in the upper few centimeters of specific samples (Pl. 52/1c-1h). Band formation begins by the aggregation of grey clotted micrite in surface mats (Pl. 52/1c, 1d). The clotted micrite is confined to specific portions of the mat: an organic mat framework defines the intervening spaces between clotted laminae. Below the surface, the micritic bands lack an organic framework, but retain the open pore spaces originally occupied by mat (Pl. 52/1e, 1f). These laminae may be heavily encrusted with worm tubes.

Eventually, open spaces within the clotted laminae are infilled with additional micritic carbonate, to form dense bands (Pl. 52/1g, 1h). Infilling carbonate often has a dark, micropeloidal texture (Pl. 52/1h) and may include red-brown clotted micrite. Small cavities are commonly infilled with aragonite needle cement. Foraminifera and worm tubes in inter-band pore spaces may be incorporated into the micritic bands as infilling progresses.

SEM observations (Pl. 51/2) indicate that the micrite in the uppermost layers, where evidence of a microbial mat is seen in thin section, consists of equant to elongate crystals less than 1 µm in size; these crystals are embedded in organic gel matrix (Pl. 51/2b). Crystals in the lower, denser layers are similar in size and shape, but organic films are minimal to absent. Microborings are locally abundant, but much of the banded micrite shows no evidence of boring.

Distribution: LM forms the upper caps of subtidal stromatolites 858, 79-135.4 and 857 (Fig. 3). In 858, LM grades downward to a transitional micrite-calcarenite microfabric. In 79-135.4 and 857, LM grades downward to unlaminated micrite. As previously noted, although no mat was observed

Plate 50 Hamelin Pool stromatolites (Western Australia). Massive Micrite (MaM) microfabric.

Fig. 1a. Vertical section through a slabbed field specimen showing characteristic dense, massive texture, mottled greenish to light brown color, and knobby upper surface (arrows). Bivalve shells (s) are common. Sample 842.

Fig. 1b. Low magnification photomicrograph showing dense microcrystalline carbonate with irregular pores and radial and convex upward cracks; some cracks are filled or partially filled with internal sediment (arrows). Thin section SB-99-4.

Figs. 1c, 1d. Gradation from dense, homogenous micrite to more open, equant clusters. Note the characteristic golden to red-brown color of the micrite. Detail of boxed area in 1c is shown in 1d. Thin section 842-B.

Fig. 1e. Golden micrite with small black inclusions; filament molds (arrows) are scattered throughout the micrite. Thin section SB-99-4.

Fig. 1f. Golden micrite with granular texture; outlines of granules are defined by dark micritic coatings (d) and overlying aragonite needle cement (an). Thin section 842-D.

Fig. 1g. Carbonate sand grains (right) infilling a cavity within a massive micrite framework (left); a red-brown micritic matrix extends between the grains of internal sediment (arrow). These sediment-rich areas form the light brown patches seen in hand specimens (Fig. 1a). Thin section 842-C.

Fig. 1h. Micritization of foraminifera in cavity fill; note progression from fresh (1), to partly altered (2), to completely micritized (3) skeletons. Thin section 842-C.

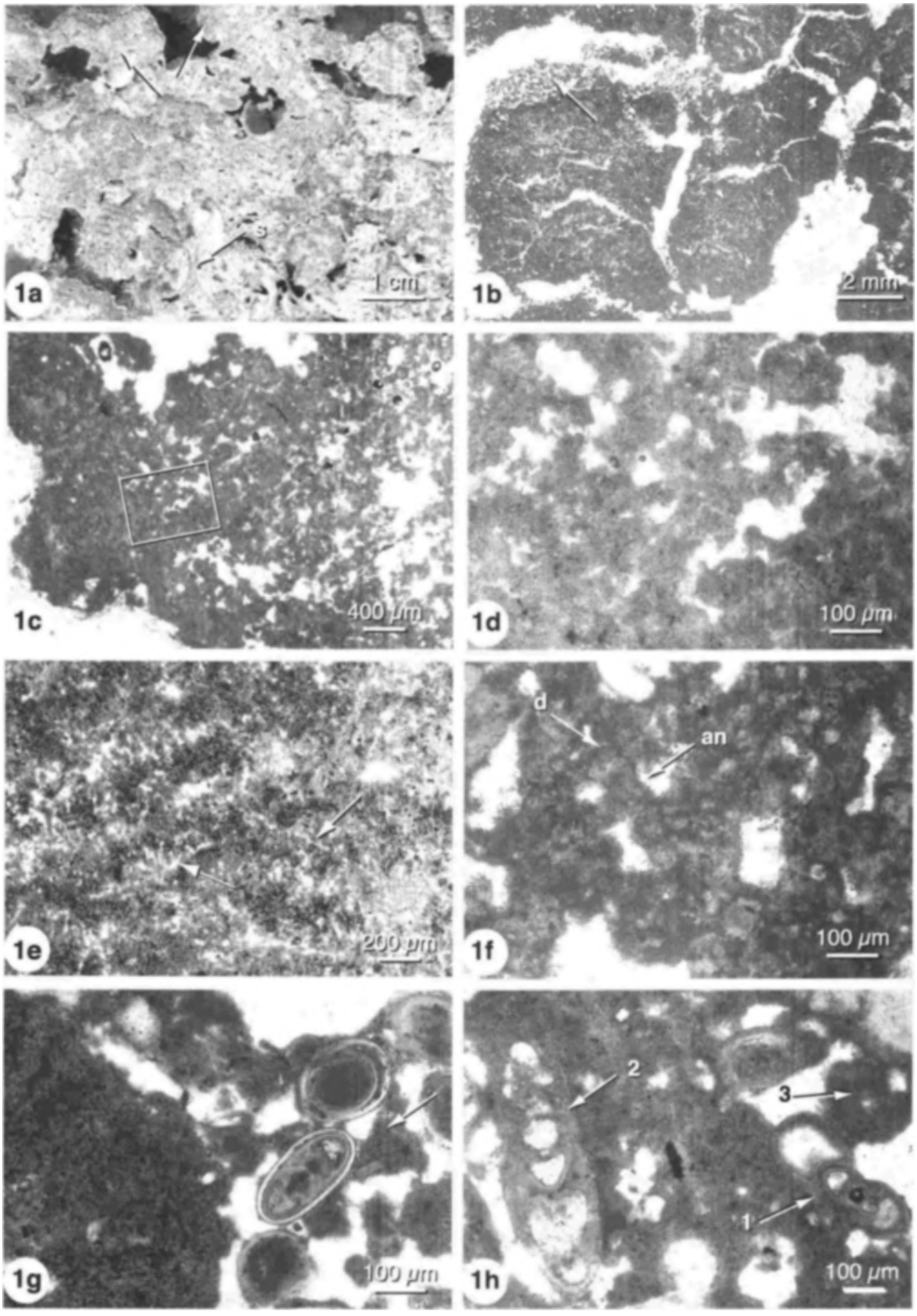
1a
1 cm
1b
2 mm
1c
400 µm
1d
100 µm
1e
200 µm
d
an
1f
100 µm
1g
100 µm
2
3
1
1h
100 µm

at the top of 857 during field collection, thin section observations indicate the presence of an organic mat embedded with micrite in the uppermost 2 mm of this sample.

Origin: Laminated micrite is interpreted as a primary depositional microfabric formed in the subtidal zone by an unknown mat type. Observations of clotted micrite within an organic mat framework (Pl. 52/1c, 1d) at the surface of some stromatolites exhibiting the LM texture are evidence that microbial mats are involved in micrite accretion. Interband porosity, present as large laminoid fenestrae (Pl. 52/1a, 1b), represents space originally occupied by the organic framework of the accreting mat (Pl. 52/1c, 1d). Preservation of the organic matter as observed in thin sections is poor and the composition of the accreting mats is unknown.

SEM observations showing a lack of grain outlines and a paucity of microboring in surface micrite bands (Pl. 52/2a) are evidence that the clotted micrite is not trapped and bound peloids or microbored grains, but instead is precipitated within the mat. Further evidence for organically induced precipitation of micrite within the surface bands is the close association between crystals and organic gel (Pl. 51/2b), with a downward loss of gel in the subsurface (Pl. 51/2d).

The increasing density of micrite, from relatively open surface bands (Pl. 52/1e, 1f) to dense subsurface bands (Pl. 52/1g, 1h) indicates that precipitation of micrite continues in the subsurface. The mechanism of subsurface precipitation is unknown, but the dark micropeloidal textures of the infilling micrite (Pl. 52/1h) are suggestive of precipitation in an organic matrix (e.g. Dupraz and Strasser 1999, 2002).

4.2.3 Unlaminated Micrite (UM, Pl. 53)

Unlaminated micrite is characterized by irregular dense limestone with an irregular fenestral fabric. Slabbed specimens show a network of dense limestone with abundant cm- to mm-sized open fenestrae (Pl. 53/1a); some fenestrae are filled with chalky sediment. Low magnification photomicrographs show mottled carbonate with irregular cavities (Pl. 53/1b). Chalky areas of loose sediment may have been lost during the thin sectioning process.

Higher magnification photomicrographs reveal a pattern of micritic bands (Pl. 53/1c, 1d). These bands are identical to those described in the laminated micrite fabric above. The banded structure is altered to an unlaminated fabric by partial infilling of pore spaces between the bands. Pore spaces are infilled with dark peloidal micrite, red-brown clotted micrite, and aragonite needle cements (Pl. 53/1e-1g); needle cements commonly radiate in fan-shaped bundles from cavity walls.

Skeletal grains and ooids in the pore spaces are incorporated into the enveloping micrite network. These grains are often extensively micritized, eventually loosing all definition of their origin (Pl. 53/1h).

Distribution: Unlaminated micrite is the dominant microfabric in subtidal stromatolites 79-135.4, 844, and 843 and is present in 857 (Fig. 3). UM grades upward to LM in 79-135.4 and 857. In 857, UM grades downward to micrite-calcarenite (M-C) transitional microfabric. In 843, UM overlies unlaminated calcarenite; the nature of this transition is unknown, as it was not sampled in thin section and is not apparent in hand sample.

Plate 51 Hamelin Pool stromatolites (Western Australia).

Part 1. Massive Micrite (MaM) microfabric; all except Fig. 1a are SEMS images.

Fig. 1a. Scanned image of a vertical thin section through a knobby surface crust in transmitted light; a microcrystalline carbonate framework is dissected by convex upward and radial cracks filled or partially filled with internal sediment. Arrows indicate the location of Figs. 1b, 1c and 1d. Thin section SB-99-4.

Fig. 1b. Globular to ovoid sub-micron crystals embedded in organic gel at the uppermost surface of the knobby crust.

Fig. 1c. Irregular elongate sub-micron crystals with patches of film two millimeters below the surface.

Fig. 1d. Rod and needle-shaped crystals up to 1 µm long lacking organic gel 2.5 cm below the surface of the knobby crust; EDS analyses showing 1-2% Sr in these crystals support XRD analysis of bulk samples indicating aragonite.

Part 2 SEM images of Laminated Micrite (LM) microfabric.

Fig. 2a. Micritic lamina near the surface of subtidal stromatolite 858; a petrographic microscope view of this area is shown in Pl. 52/1d. An organic mat framework (om) defines laminar pore space on either side of the micritic band. The micrite has a clotted texture with open pore spaces between the clots. Arrow indicates the location of Fig. 2b. Thin section 858-A

Fig. 2b. Sub-micron irregular crystals (< 1 µm), embedded in organic gel. EDS analyses suggest aragonite.

Fig. 2c. Dense micritic lamina 1 cm below the surface of subtidal stromatolite 858. Arrow marks the location of Fig. 2d. Thin section 858-A

Fig. 2d. Heterogeneous mixture of sub-micron irregular crystals with little to no organic gel. EDS analyses suggest an aragonite composition.

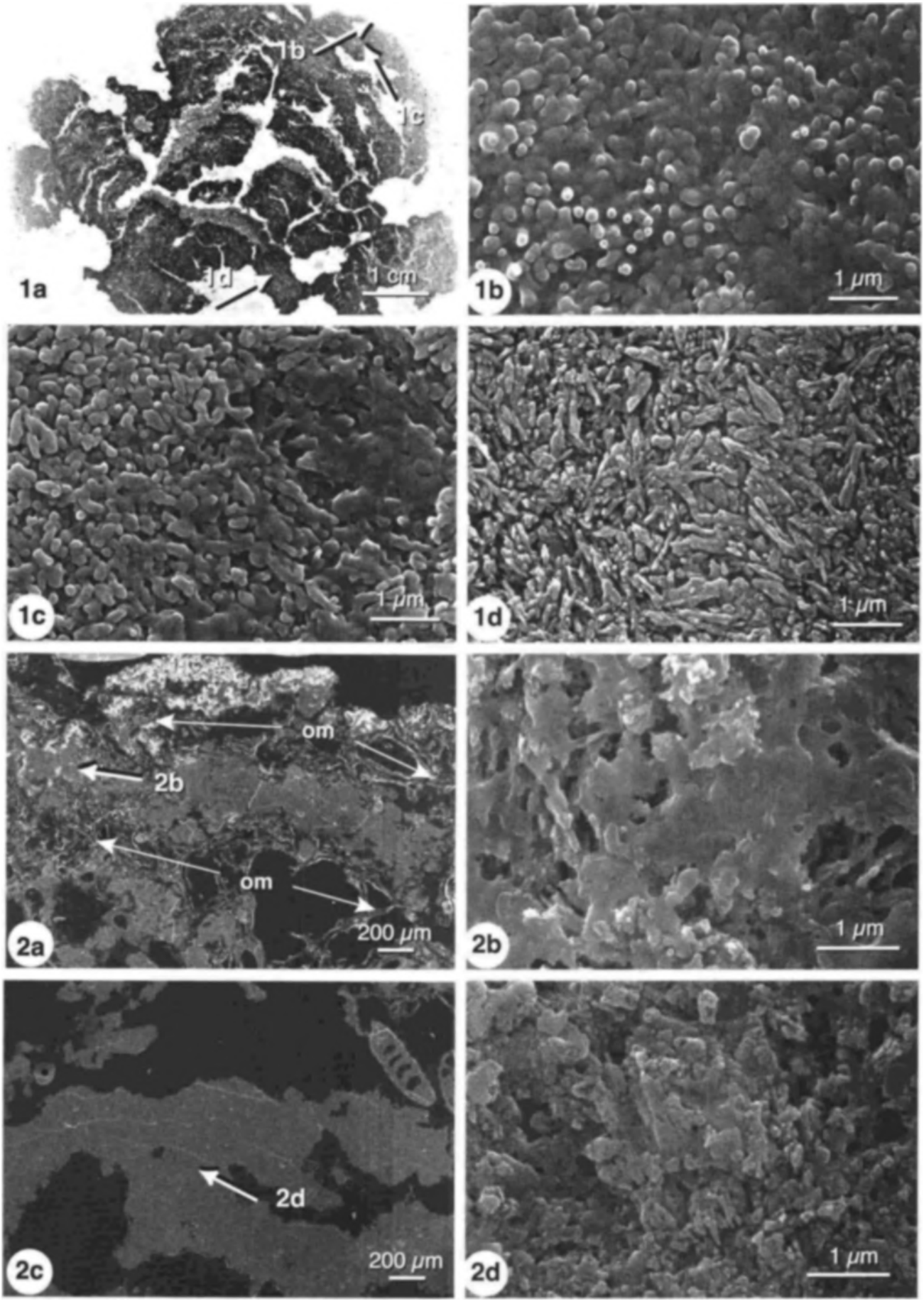
1a
1b
1c
1d
1 cm
1b
1 μm
1c
1 μm
1d
1 μm
2a
om
2b
om
200 μm
2b
1 μm
2c
2d
200 μm
2d
1 μm

Origin: Unlaminated micrite is interpreted as a diagenetic microfabric formed by alteration of laminated micrite. Alteration results from aragonite precipitation in the large laminoid fenestrae that comprise LM inter-band porosity (Pl. 53/1c-1f). This precipitation obliterates pore space and transforms the banded structure to an irregular fenestral fabric (Pl. 53/1b). Petrographic features of the interband precipitates, such as dark micropeloidal micrite (Pl. 53/1d, 1f) and golden granules (Pl. 53/1g) fringed with aragonite needle cement (Pl. 53/1d, 1f, 1g, 1h), are characteristic of precipitates formed in *Entophysalis* mats, as described in MaM and LC-1. *E. major*, the dominant component of the intertidal pustular mats forming MaM and LC-1 does not grow well in subtidal environments (Golubic 1983). However, a subtidal coccoid entophysalidecean cyanobacterium that is new to science has been reported as a dominant component of gelatinous colloform mats (Golubic 1992); this species, which has not yet been described (S. Golubic, pers. comm. 2003), may be important in the precipitation of interband micrite and thus the formation of the UM microfabric. Gradual obliteration of internal structure of skeletal grains within UM (e.g. Pl. 53/1h) may be the result of microboring and micritization by *Solentia*.

The continuum from laminated to unlaminated micrite in samples 79-135.4 and 857 (Fig. 3) is consistent with the interpretation that the UM microfabric forms by progressive alteration of a primary banded structure. The occurrence of UM at the top of samples 843 and 844 suggests that these stromatolites are not presently colonized by mats precipitating banded micrite.

4.3 Micrite-Calcarenite Transitional Microfabric (M-C)

The M-C microfabric is transitional between the end-members described above. It is similar to unlaminated micrite, but calcarenite, rather than micrite infills the micrite bands (Pl. 47/2a). With progressive infilling by calcarenite, the micritic bands become increasing difficult to recognize, and the microfabric grades to unlaminated calcarenite (Pl. 47/2b). Sand grains in the calcarenite infillings are characterized by dark, micropeloidal coatings, golden granules, and aragonite needle cement (Pl. 47/2a, 2b)

Distribution: M-C microfabric forms the dominant component of stromatolite 858 in the shallow subtidal zone (Fig. 3). At the top of this stromatolite, M-C grades upward to laminated micrite (LM). In addition, in subtidal stromatolite 857, unlaminated micrite (UM) grades to M-C, which in turn grades downward to unlaminated calcarenite (UC).

Origin: Like UM, the transitional micrite-calcarenite microfabric is interpreted as a diagenetic alteration of laminated micrite. Observation of micritic bands in some thin sections (Pl. 47/2a) is evidence of the original laminated structure. Infilling of laminoid fenestrae with sand (Pl. 47/2a, 2b) rather than micritic precipitates suggests frequent sediment influx, or possible burial. Dark, micropeloidal coatings and golden granules fringed with aragonite needle cement in the calcarenite infillings (Pl. 47/2a, 2b), which are characteristic of *Entophysalis* precipitation, suggest an active presence by a subtidal entophysalidecean community in the interband porosity. Stromatolite 858, composed mainly of M-C, is in a sense a hybrid between subtidal stromatolites, which are predominantly micritic, and intertidal stromatolites, composed mainly of calcarenite.

5 SYNTHESIS

5.1 Role of Microbes

The microfabrics in Shark Bay stromatolites are manifestations of four basic components: carbonate sand accumulated through microbial trapping and binding, and three products of microbial precipitation: (a) fused, micritized grains, (b) a 'triumvirate' of dark, micropeloidal micrite, golden to red-brown micrite, and fringing aragonite needle cement, referred to henceforth as the 'golden micrite triumvirate' and (c) clotted micrite laminae. These components combine to form distinct microfabrics, which in turn form a variety of stromatolite types (Fig. 4). Accumulation of each component is a function of microbial activity as follows:

Carbonate sand is trapped and bound by smooth mats composed of filamentous cyanobacteria, such as *Schizothrix* or *Microcoleus*, and by pustular coccoid cyanobacterial mats formed by *Entophysalis major*. Grains are typically fresh, with well-preserved internal structure. Trapped and

Plate 52 Hamelin Pool stromatolites (Western Australia). Laminated Micrite (LM) microfabric.

Fig. 1a. Vertical section through a slabbed field specimen showing bands of dense, light colored limestone and interband porosity. Sample 858.

Fig. 1b. Low magnification photomicrograph showing laterally continuous micritic bands 200 μm to 2 mm thick separated by open pore space. Thin section 79-135.4.

Figs. 1c, 1d. Upper surface of stromatolite 858 shown in Fig. 1a. Grey clotted micrite forms distinct bands or laminae within a microbial mat. Interband spaces are defined by organic components of the mat (om). Thin section 858-A.

Fig. 1e. Near surface band, lacking organic framework; note the complex open structure. Boxed area is shown in Fig. 1f. Thin section 79-135.4.

Fig. 1f. Detail of Fig. 1e showing the clotted texture of the micritic layer. Thin section 79-135.4.

Fig. 1g. Subsurface layer of dense, clotted micrite. Boxed area is shown in Fig. 1h. Thin section 79-135.4.

Fig. 1h. Detail of Fig. 1g showing the dense clotted micritic texture of this band; the color patterns suggest infilling of an open structure, such as that in Fig. 1f, by a second generation of darker clotted to micropeloidal micrite (arrow). Thin section 79-135.4.

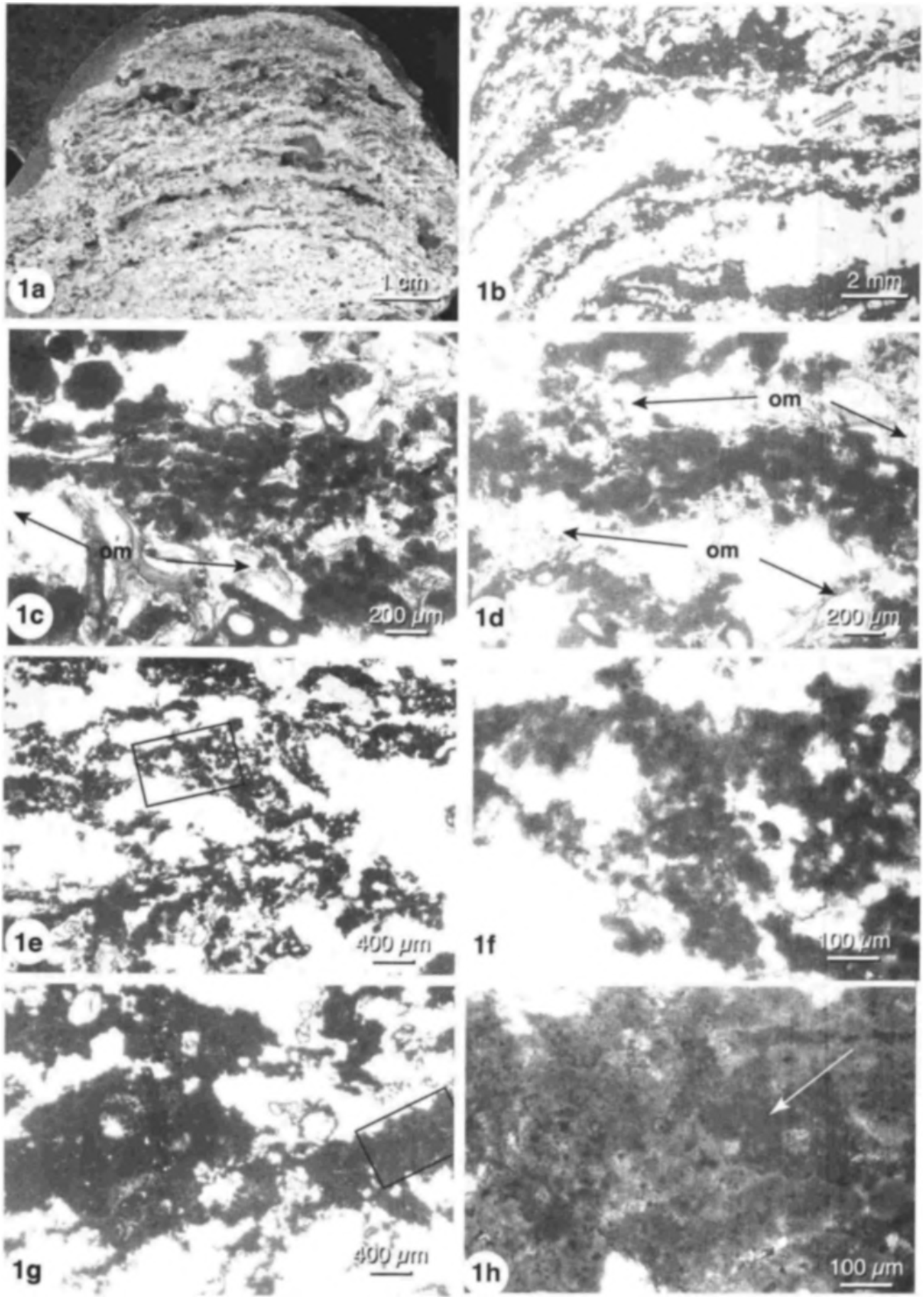
1a
1 cm
1b
2 mm
1c
om
200 µm
1d
om
om
200 µm
1e
400 µm
1f
100 µm
1g
400 µm
1h
100 µm

bound sand forms the accretionary framework of LC-1, LC-2, and UC (Fig. 4).

Fused micritized sand grains are formed as a result of endolithic activity by the coccoid cyanobacterium *Solentia* sp. Syndepositional precipitation of micrite in organic gel within *Solentia* boreholes crossing between grains leads to grain fusion. Grain fusion by micritization lithifies trapped and bound sediment, forming cemented layers in LC-2 and irregular patches in UC; fused micritized grain layers may also be present in LC-1.

The 'golden micrite triumvirate' of dark micropeloidal micrite and golden to red brown micrite coated with aragonite needle cement is formed as a result of calcification of *Entophysalis* mats (intertidal *Entophysalis major* and probably also a subtidal entophysalidecean species). The aragonite needles represent abiotic precipitation templated on *Entophysalis* precipitates and are a characteristic feature of these mat precipitates. Golden micrite triumvirate lithifies trapped and bound sediment, forming cemented layers in LC-1 and irregular cemented patches in UC. In addition, the golden micrite element of the triumvirate forms the accretionary framework of MaM, and triumvirate infills laminoid fenestrae in UM.

Clotted micrite laminae are formed by precipitation within an unknown subtidal mat type. These laminae form the primary accretionary framework of LM and UM.

Interactions between microbial communities result in the combination of components to form distinct microfabrics as follows:

LC-1 is formed by a cycling between smooth mats (*Schizothrix* or other filamentous cyanobacteria) and pustular mats composed mainly of *Entophysalis major*. The smooth mats trap and bind sand; *Entophysalis* mats trap and bind sand and calcify, precipitating golden triumvirate in interstial pore space. The result is layered couplets of uncemented sand and sand cemented by triumvirate.

LC-2 is formed by a cycling between smooth mats (*Schizothrix* or other filamentous cyanobacteria) and endolithic communities of *Solentia* sp. The smooth mats trap and bind sand; *Solentia* micritizes sand grains, which become welded together. The result is layered couplets of uncemented sand and sand cemented by grain fusion.

UC is formed by sediment trapping and binding and episodic calcification of pustular *Entophysalis* mats. The result is an irregular mixture of sand and golden micrite triumvirate.

MaM is formed by lithification of mats comprised solely of *E. major*, with little to no incorporated sediment. The result is a framework of golden micritic aragonite.

LM is formed by an unknown mat type that precipitates bands of clotted micritic aragonite. The result is a laminated micritic framework.

UM is formed by precipitation of golden triumvirate by an undescribed entophysalidecean community within the laminoid fenestrae of LM. The result is obliteration of lamination to form an unlaminated micritic framework.

Distributions of microbes within the peritidal environment determine the spatial patterns of microfabric and stromatolite structure as follows:

Upper intertidal to supratidal zone: This zone is characterized by laminated stromatolites composed mainly of LC-1 (Fig. 4). LC-1 is interpreted to form by alternation of *Schizothrix* and *Entophysalis* mats in the lower intertidal zone, suggesting that these stromatolites formed when sea level was higher than it is today.

Mid to lower intertidal zone: Unlaminated stromatolites composed mainly of UC, with caps of MaM, form in this zone. This reflects the formation of UC in pustular *Entophysalis* mats in mid to lower tidal zones and MaM in topographically higher *Entophysalis* mats, with reduced sediment influx.

Lower intertidal to shallow subtidal zone: Two types of laminated stromatolite form in this zone. Larger buildups consist of LC-1, representing an alternation between filamentous and *Entophysalis* mats. Smaller buildups consist of LC-2, formed by cycling between filamentous and endolithic cyanobacteria. These differences may be related to exposure frequency.

Subtidal: Laminated to unlaminated stromatolites in this zone are composed of LM grading to UM. Lamination results from precipitation of micritic laminae in subtidal microbial mats of unknown composition; diagenetic infilling of open fenestrae between the micritic bands by a subtidal entophysalidecean species obliterates original lamination.

Plate 53 Hamelin Pool stromatolites (Western Australia). Unlaminated Micrite (UM) microfabric.

Fig. 1a. Vertical section through a slabbed field specimen showing a network of dense carbonate with abundant small fenestrae. Sample 844.

Fig. 1b. Low magnification photomicrograph of the specimen in Fig. 1a, showing the dense micritic network and small irregular pores. Thin section 844-A.

Figs. 1c-1f. Higher magnification photomicrographs showing that the dense carbonate networks are comprised of micritic bands infilled with dark, micropeloidal micrite (mp) and aragonite needle cement (an). Boxed area in 1c is shown in 1d; boxed area in 1g is shown in 1f. Figs. 1c, 1d: thin section 79-135.4; Figs 1e, 1f: thin section 844-D.

Fig. 1g. High magnification photomicrograph of a cavity fill showing golden granular micrite (arrows) infilling pore space between bivalve shells (s); granules are rimed with dark micrite and coated with fringe cement. Thin section 843-B.

Fig. 1h. Micritized foraminifera (f) and micropeloidal micrite (arrow) infilling interband porosity; extensive micritization can obliterate evidence of skeletal origin, forming micritic peloids. Thin section 844-B.

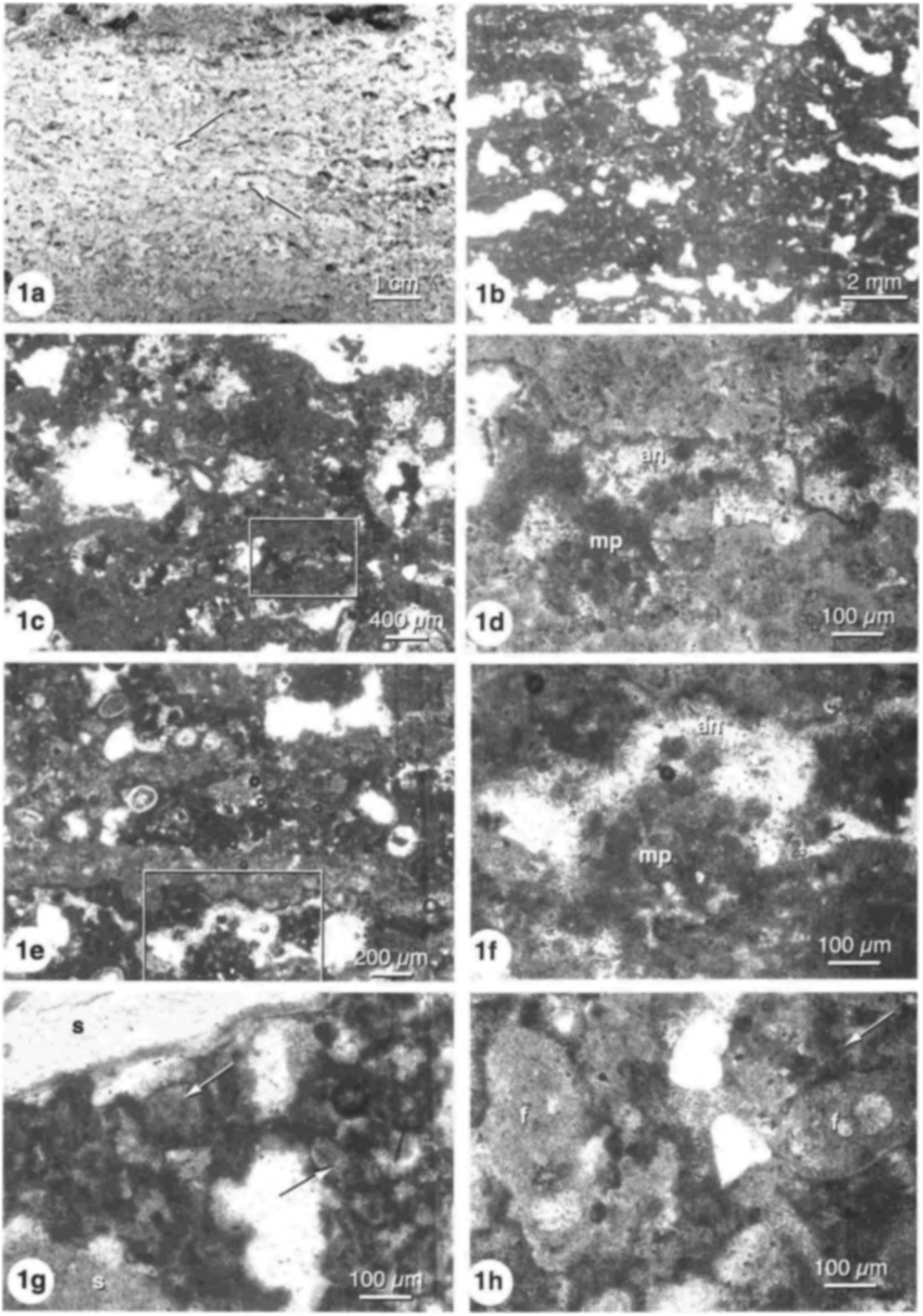
1a
1 cm
1b
2 mm
1c
400 µm
1d
arr
mp
100 µm
1e
200 µm
1f
arr
mp
100 µm
1g
s
s
100 µm
1h
f
f
100 µm

5.2 Comparison with Previous Ideas

Our detailed study of microfabric sheds new light on the origins of Shark Bay stromatolites. In contrast to previous reports, which ascribe accretion of Hamelin Pool stromatolites to trapping and binding of sediment (Playford 1990; Golubic 1992; McNamara 1999), we recognize two fundamentally different structures: (1) grainy, calcarenite stromatolites, with primary accretion by sediment binding and trapping and (2) muddy, micritic stromatolites with primary accretion resulting from *in situ* precipitation of microcrystalline aragonite (Fig. 4). Recognition of micritic stromatolite buildups in Shark Bay is of fundamental importance as many ancient stromatolites are micritic.

Comparison of Figs. 2 and 4 shows some similarities but also significant differences between our results, based on microfabric, and previous interpretations, based mainly on stromatolite macrostructure. Previous studies have described stromatolites in the upper to mid intertidal zone (Pustular-Mat Stromatolites of Playford 1990) as unlaminated structures built by *Entophysalis* mats (Logan et al. 1974; Hoffman 1976; Playford and Cockbain 1976). This is, in part, consistent with our interpretation that *Entophysalis* mats form unlaminated buildups of UC capped with MaM in the mid intertidal zone (Fig. 4). Our results, however, also show laminated (rather than unlaminated) stromatolites in the upper intertidal zone. These emergent laminated forms are interpreted as relict structures formed in the lower intertidal zone during higher sea level stands. These results support previous speculation that some intertidal forms are relict (Playford and Cockbain 1976; Burne and James 1986; Chivas et al. 1990).

Laminated stromatolites in the lower intertidal to shallow subtidal zones, designated 'Smooth-Mat Stromatolites' by Playford (1990), have previously been interpreted as products of trapping and binding by smooth filamentous cyanobacterial mats, which were cemented a few millimeters below the surface (Logan 1961, Logan et al. 1974; Hoffman 1976; Playford and Cockbain 1976). Logan (1961) suggested that lithification occurred by abiotic cementation when the structures were exposed. Others (e.g. Playford 1979, 1990) speculated that it was likely that algal or bacterial action were involved in lithification. Our analysis of microfabric in lower intertidal to shallowest subtidal stromatolites provides evidence for two types of laminated calcarenite buildups, both of which form by an alternation between microbial trapping and binding and microbial precipitation (Fig. 4). The most common type, the LC-1 stromatolites of Fig. 4, are formed by a cycling between smooth mats and pustular *Entophysalis* mats; early lithification results from calcification of pustular mats. The second type, which forms the smaller laminated LC-2 stromatolites of Fig. 4, are formed by a cycling between filamentous cyanobacteria and endolithic communities; early lithification results from fusion of micritized grains. Recognition of microbial micritization as a mechanism of of stromatolite lithification contrasts with previous ideas that endolithic activity serves only to weaken and destroy the stromatolites (e.g. Golubic 1992).

Subtidal stromatolites were previously described as weakly laminated and designated as 'Colloform Mat Stromatolites' (Playford 1990). Accretion was attributed to trapping and binding of sediment in soft, coherent colloform mats composed of diverse cyanobacteria and diatoms, with lithification a few millimeters or centimeters below the surface (Playford and Cockbain 1976; Hoffman 1976, Playford 1990). Subtidal stromatolites with hard surfaces were considered to be inactive (Playford and Cockbain 1976). Our results are quite different. Microfabric analyses indicate that the dominant accretionary framework in the subtidal stromatolites examined for this study is aragonitic micrite formed by microbial precipitation (Fig. 4). This micrite is precipitated in a microbial mat of unknown composition, forming a laminated structure of aragonite bands and open pore space. The laminoid fenestrae, representing pore space originally occupied by the mat, are subsequently infilled with micrite precipitated by a subtidal entophysalidecean species, leading to a gradual loss of lamination.

6 CONCLUSIONS

1. Hamelin Pool stromatolites are formed by (a) microbial trapping and binding and (b) microbial precipitation. Microbial trapping and binding is the primary accretionary mechanism in the intertidal zone, forming grainy, calcarenite stromatolites. Microbial precipitation is the primary accretionary mechanism in the subtidal zone, forming muddy, micritic stromatolites. Microbial precipitation also cements trapped and bound sediment in the calcarenite stromatolites.

2. Micritic stromatolites in the subtidal zone have an initial laminated fabric, formed by precipitation of bands of micritic aragonitic in surface microbial mats of unknown composition. Additional precipitation of micritic aragonite by a subtidal entophysalidecean cyanobacterium infills laminoid pore space originally occupied by the mat and obliterates lamination.

3. Calcarenite stromatolites in the lower intertidal zone include two types of laminated structures; in both types, lamination represents layered couplets of cemented and uncemented sand. In Type 1, cemented layers are formed by calcification of thin *Entophysalis* mats. In Type 2, cemented layers are formed by grain fusion resulting from microbial micritization by *Solentia* sp. Uncemented layers in both types are accreted by microbial trapping and binding. Type 2 laminated calcarenite stromatolites are similar to Bahamian stromatolites in Exuma Cays.

4. Calcarenite stromatolites in mid to upper intertidal zones are unlaminated buildups formed by trapping and binding of sand by soft pustular *Entophysalis* mats; accreted sediment is lithified by precipitation of micritic cement during intervals of mat calcification.

5. Laminated calcarenite stromatolites presently occupying the upper intertidal zone are relict structures that formed in the lower intertidal zone when sea level was higher than present.

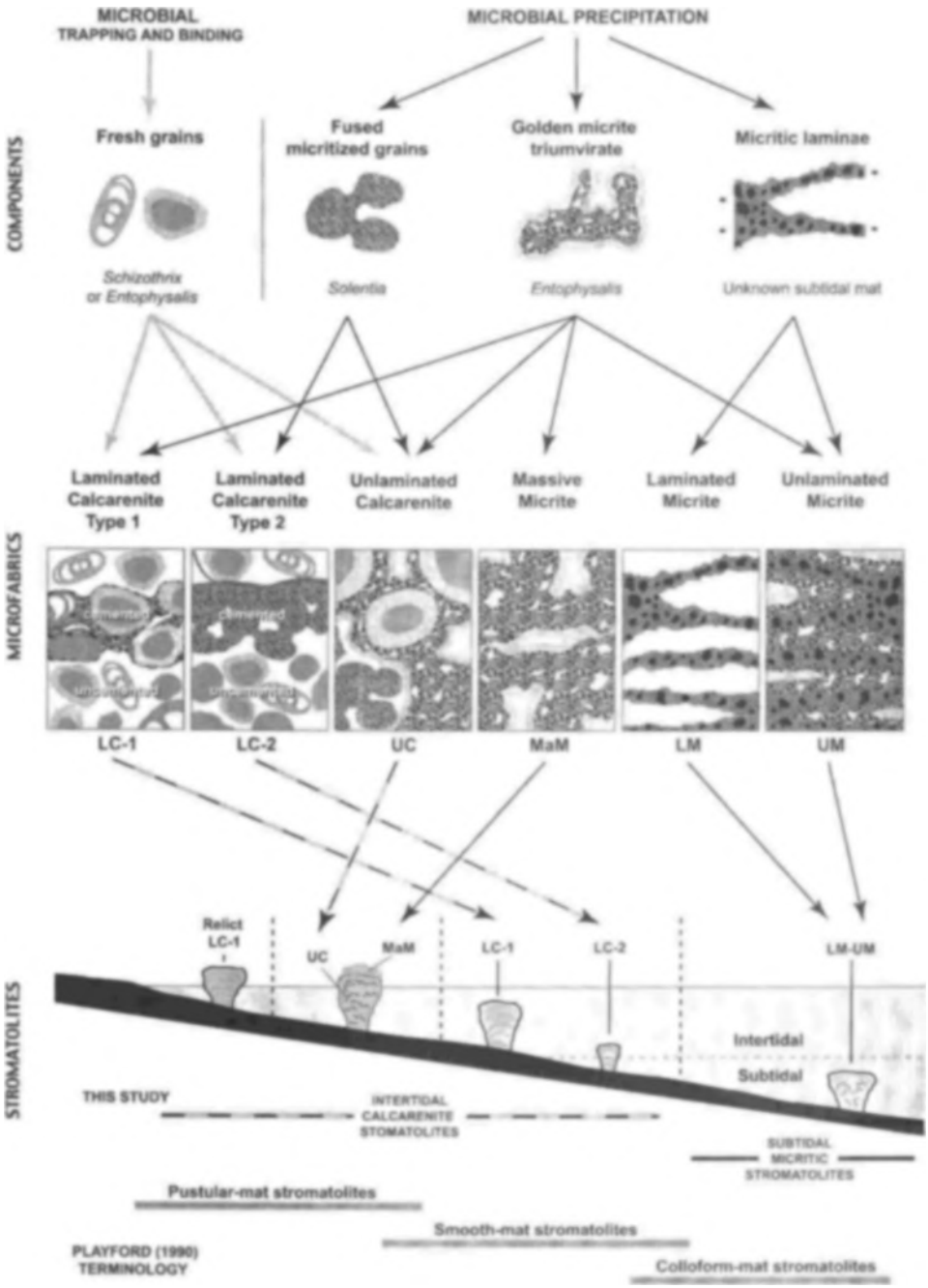

Fig. 4. Schematic diagram summarizing results of this study. Microbial trapping and binding (grey arrows) and microbial precipitation (black arrows) form individual components, microfabrics, and stromatolite buildups in Hamelin Pool; dashed arrows indicate combined trapping and binding and microbial precipitation. Calcarenite stromatolites are grainy; micritic stromatolites are muddy. Arrow is not drawn from LC-1 microfabric to the relict LC-1 stromatolite (bottom left) to emphasize that LC-1 does not form in the upper intertidal zone. See Chap. 5 for further explanation.

6. Detailed geomicrobiological studies are needed to identify specific microbial populations and processes forming the observed microfabrics.

ACKNOWLEDGEMENTS

We are grateful to P. E. Playford and J.W. Fell for logistical assistance in 1999 (R.P.R); R. N. Ginsburg for samples collected in 1979; D. Dean for outstanding thin section preparation (1979 and 1999 samples), and S. Golubic for discussion regarding *Entophysalis* calcification. Funding was provided by the Natural Sciences and Engineering Research Council of Canada (N.P.J) and the U.S. National Science Foundation (R.P.R.). The Western Australia Dept. of Conservation and Land Management granted a sample permit in 1999 (R.P.R.). Research Initiative on Bahamian Stromatolites (RIBS) Contribution # 25.

REFERENCES

Awramik, S.M. and Riding, R. (1988): Role of algal eukaryotes in subtidal columnar stromatolite formation. – Proceeding of National Academy of Science, USA, **85**, 1327-1329.

Bauld, J. (1984): Microbial mats in marginal marine environments: Shark Bay, Western Australia, and Spencer Gulf, South Australia. – In: Castenholz, R.W., Cohen, Y. and Halvorson, H.O.

(eds.): Microbial Mats: Stromatolites – 9-58, New York (Liss).
Burne, R.V. (1992): Lilliput's Castles - Stromatolites of Hamelin Pool. – Landscope-WA's Conservation, Forrests and Wildlife Magazine, 772, 34-40. CALM. WA
Burne, R.V. and Hunt, G. (1990): The Geobiology of Hamelin Pool. – Bureau of Mineral Resources, Australia, Record 1990/89. 288 pp.
Burne, R.V and James, N.P. (1986): Subtidal origin of club-shaped stromatolites, Shark Bay. Abstracts 12th Int. Sedimentol. Cong., p. 49, Canberra.
Burne, R.V. and Moore, L. S. (1987): Microbialites: organo-sedimentary deposits of benthic microbial communities. – Palaios 2, 241-254.
Chivas, A.R., Torgersen, T. and Polach, H.A. (1990): Growth rates and Holocene development of stromatolites from Shark Bay, Western Australia. – Australian Journal of Earth Science, **37**, 113-121.
Dupraz, C. and Strasser, A. (1999): Microbialites and micro-encrusters in shallow coral bioherms (Middle to Late Oxfordian, Swiss Jura Mountains). – Facies, **40**, 101-130.
Dupraz, C. and Strasser, A. (2002): Nutritional Modes in Coral-Microbialite Reefs (Jurassic, Oxfordian, Switzerland): Evolution of Trophic Structure as a Response to Environmental Change. – Palaios, **17**, 449-471.
Garret, P. (1970): Phanerozoic stromatolites: noncompetitive ecologic restriction by grazing and burrowing organisms. Science, **169**, 171-173.
Golubic, S. (1976): Comparison of Holocene and mid-Precambrian Entophysalidaceae (Cyanophyta) in stromatolitic algal mats: cell division and degradation. – Jour. Paleontology, **50**/6, 1074-1082.
Golubic, S. (1983): Stromatolites, fossil and Recent: a case history. – In: Westbroek, P. and de Jong, E.W. (eds): Biomineralization and Biological Metal Accumulation. – 313-326, Dordrecht (Reidel).
Golubic, S. (1985): Microbial mats and modern stromatolites in Shark Bay, Western Australia. – In: Cardwell, D.E., Brierley, J.A., and Brierley, C.L. (eds): Planetary Ecology. – 3-16, New York (van Nostrand).
Golubic, S. (1992): Stromatolites of Shark Bay. – In: Margulis, L. and Olendzenski, L. (eds.): Environmental Evolution: Effects of the Origin and Evolution of Life on Planet Earth. – 131-147, Cambridge (MIT Press).
Hoffman, P. (1976): Stromatolite morphogenesis in Shark Bay, Western Australia. – In: Walter, M.R. (ed.): Stromatolites. – Developments in Sedimentology, **20**, 261-271, Amsterdam (Elsevier).
Kalkowsky, V.H.E. (1908): Oolith und stromatolith im norddeutschen Buntsandstein. – Z. Deut. Geol. Ges., **60**, 231-242.
Kawaguchi, T. and Decho, A.W. (2001): Potential roles of extracellular polymeric secretions (EPS) in regulating calcification: a study of marine stromatolites, Bahamas. – Thalassas, **17**, 11-19.
Kawaguchi T. and Decho, A.W. (2002): Isolation and biochemical characterization of extracellular polymers (EPS) from modern soft marine stromatolites: inhibitory effects on $CaCO_3$ precipitation. – Preparative BioChemistry BioTechnology, **32**, 51-63.
Logan, B.W. (1961): *Cryptozoon* and associate stromatolites from the Recent Shark Bay, Western Australia. – Journ. Geology, **69**, 517-533.
Logan, B.W. and Cebulski, D.E. (1970): Sedimentary environments of Shark Bay, Western Australia. – In: Carbonate Sedimentation and Environments, Shark Bay, Western Australia. – Amer. Assoc. Petrol. Geol. Mem., **13**, 1-37.
Logan, B.W., Hoffman, P. and Gebelein, C.D. (1974): Algal mats, cryptalgal fabrics and structures, Hamelin Pool, Western Australia. – In: Evolution and Diagenesis of Quaternary Carbonate Sequences, Shark Bay, Western Australia. – Amer. Assoc. Petrol. Geol. Mem., **22**, 140-194.
Logan, B.W., Read, J.F, and Davies, G.R. (1970): History of carbonate sedimentation, Quaternary Epoch, Shark Bay, Western Australia. – In: Carbonate Sedimentation and Environments, Shark Bay, Western Australia. – Amer. Assoc. Petrol. Geol. Mem., **13**, 38-84.
Logan, B.W., R. Rezak, and R.N. Ginsburg (1964): Classification and environmental significance of algal stromatolites. – Journal of Geology, **72**, 68-83.
Hagan, G.M. and Logan, B.W. (1974): Development of carbonate banks and hypersaline basins, Shark Bay, Western Australia. In: Evolution and Diagenesis of Quaternary Carbonate Sequences, Shark Bay, Western Australia. – Amer. Assoc. Petrol. Geol. Mem., **22**, 61-139.
Macintyre, I.G., Prufert-Bebout, L. and Reid, R.P. (2000): The role of endolithic cyanobacteria in the formation of lithified laminae in Bahamian stromatolites. – Sedimentology, **47**, 915-921.
McNamara, K. (1999): Stromatolites. – 28p. Western Australian Museum, Perth.
Monty, C.L.V. (1973): Precambrian background and Phanerozoic history of stromatolitic communities, an overview. – Annales de la Société Géologique de Belgique, **96**, 585-624.
Monty, C.L.V. (1976): The origin and development of cryptalgal fabrics. – In: Walter, M.R., (ed.), Stromatolites.– Developments in Sedimentology, **20**, 193-259, Amsterdam (Elsevier).
Playford, P.E. (1979): Stromatolite research in Western Australia. – J. Royal Soc. Western Australia, **62**/1-4, 13-20.
Playford, P.E. (1980): Environmental controls on morphology of modern stromatolites at Hamelin Pool, Western Australia. – West. Aust. Geol. Survey Ann. Rept. (for 1979), 73-77.
Playford, P.E. (1990): Geology of the Shark Bay area, Western Australia. – In: Berry, P.F., Bradshaw, S.D., and Wilson, B.R., (eds.): Research In Shark Bay. – 13-31, West Australian Museum.
Playford, P.E., and Cockbain, A. E., (1976): Modern algal stromatolites at Hamelin Pool, a hypersaline barred basin in Shark Bay, Western Australia. – In: Walter, M.R., (ed.): Stromatolites. – Developments in Sedimentology, **20**, 389-411, Amsterdam (Elsevier).
Reid, R.P., Macintyre, I.G. and Steneck, R.S. (1999): A Microbialite/algal ridge fringing reef complex, Highborne Cay, Bahamas. – Atoll Res. Bull., **466**, 1-18.
Reid, R.P., Visscher, P.T., Decho, A.W., Stolz, J.F., Bebout, B.M., Dupraz, C., Macintyre, I.G., Paerl, H.W., Pinckney, J.L., Prufert-Bebout, L., Steppe, T.F. and DesMarais, D.J. (2000): The role of microbes in accretion, lamination and early lithification of modern marine stromatolites. – Nature, **406**, 989-992.
Reid, R.P. and Macintyre, I.G. (2000): Microboring versus recrystallization: Further insight into the micritization process. – Journal of Sedimentary Research, **70**, 24-28.
Reitner, J. (1993): Modern cryptic microbialite/metazoan facies from Lizard Island (Great Barrier Reef, Australia) formation and concepts. – Facies, **29**, 2-40.
Riding, R. (1991): Classification of microbial carbonate. – In: Riding, R. (ed.), Calcareous Algae and Stromatolites. – 21-51, New York (Springer).
Riding, R. (1994): Stromatolite survival and change: The significance of Shark Bay and Lee Stocking Island subtidal columns. – In: Krumbein, W.E., Paterson, D.M., and Stal, L.J. (eds.) Biostabilization of Sediments. – 183-202, Oldenburg.
Riding, R. (2000): Microbial carbonates: the geological record of calcified bacterial-algal mats and biofilms. – Sedimentology, **47**, 179-214.
Visscher, P.T., Reid, R.P. and Bebout, B.M. (2000) Microscale observations of sulfate reduction: correlation of microbial activity with lithified micritic laminae in modern marine stromatolites. – Geology, **28**, 919-922.
Visscher, P.T., Reid, R.P., Bebout, B.M., Hoeft, S.E., Macintyre, I.G., and Thompson, J. Jr., 1998, Formation of lithified micritic laminae in modern marine stromatolites (Bahamas): the role of sulfur cycling. – American Mineralogist, **83**, 1482-1491.
Walter, M.R. and Bauld, J. (1986): Subtidal stromatolites of Shark Bay. – Abstracts 12th Int. Sedimentol. Cong., p. 315, Canberra.

Manuscript accepted September 18, 2003